# Gastric stem cells promote inflammation and gland remodeling in response to *Helicobacter pylori* via Rspo3-Lgr4 axis

Jonas Wizenty[1,2] (iD), Stefanie Müllerke[1,3], Marina Kolesnichenko[4], Julian Heuberger[1,3] (iD), Manqiang Lin[1,3], Anne-Sophie Fischer[1,2,3], Hans-Joachim Mollenkopf[5], Hilmar Berger[1], Frank Tacke[1] (iD) & Michael Sigal[1,2,3,*] (iD)

## Abstract

*Helicobacter pylori* is a pathogen that colonizes the stomach and causes chronic gastritis. *Helicobacter pylori* can colonize deep inside gastric glands, triggering increased R-spondin 3 (Rspo3) signaling. This causes an expansion of the "gland base module," which consists of self-renewing stem cells and antimicrobial secretory cells and results in gland hyperplasia. The contribution of Rspo3 receptors Lgr4 and Lgr5 is not well explored. Here, we identified that Lgr4 regulates Lgr5 expression and is required for *H. pylori*-induced hyperplasia and inflammation, while Lgr5 alone is not. Using conditional knockout mice, we reveal that R-spondin signaling via Lgr4 drives proliferation of stem cells and also induces NF-κB activity in the proliferative stem cells. Upon exposure to *H. pylori*, the Lgr4-driven NF-κB activation is responsible for the expansion of the gland base module and simultaneously enables chemokine expression in stem cells, resulting in gland hyperplasia and neutrophil recruitment. This demonstrates a connection between R-spondin-Lgr and NF-κB signaling that links epithelial stem cell behavior and inflammatory responses to gland-invading *H. pylori*.

## Introduction

*Helicobacter pylori* is a gram-negative bacterium that has evolved to colonize and persist in the stomach for decades. It is found in approx. 50% of the world's population and infection is the most important risk factor for gastric cancer. It is able to establish free-swimming colonies that survive within the protective mucus layer in direct contact with the surface epithelium (Amieva & El-Omar, 2008). In addition, a subpopulation of *H. pylori* can form colonies deep inside the gastric glands, where stem and progenitor cells reside (Sigal *et al*, 2015; Fung *et al*, 2019). It has been shown that gland-colonizing bacteria, not the bacteria colonizing the surface, induce the typical pathology associated with *H. pylori* infection, that is, stem cell expansion, gastritis, hyperplasia, and metaplasia—precursor lesions for gastric cancer (Howitt *et al*, 2011; Sigal *et al*, 2015; Fischer & Sigal, 2019; Liabeuf *et al*, 2022).

Upon attachment, highly pathogenic strains of *H. pylori* use the bacterial type IV secretion system (T4SS) to inject virulence factors into the host cell cytoplasm, including the effector molecule CagA (Backert *et al*, 2000; Amieva *et al*, 2003), as well as the LPS biosynthesis metabolite ADP-glycero-β-D-manno-heptose (ADP heptose) (Pfannkuch *et al*, 2019). ADP heptose, as well as its derivative D-glycero-β-D-manno-heptose 1,7-bisphosphate (HBP), has been shown to act as a central mediator of *H. pylori*-driven inflammation by inducing activation of the transcription factor NF-κB via alpha kinase 1 (ALPK1) and TRAF-interacting protein with forkhead-associated domain (TIFA) (Zimmermann *et al*, 2017; Pfannkuch *et al*, 2019). However, it remains unclear why these inflammatory responses are triggered specifically by bacteria that have invaded the glands and not by those that remain on the surface.

We have previously shown gland responses to *H. pylori* infection to be driven by increased expression of *Rspo3* in the stroma beneath the glands, which drives stem cell expansion and hyperplasia (Sigal *et al*, 2017). During normal gland homeostasis, a molecular signaling network established by close interplay between epithelial and stromal cells controls epithelial turnover and differentiation (Sigal *et al*, 2017; Fischer & Sigal, 2019; Kapalczynska *et al*, 2022). The antral gland base and lower isthmus contains gastric stem cells that are characterized by high Wnt signaling and expression of stem cell markers such as *Axin2* and *Lgr5* (Barker *et al*, 2010; Sigal

1 Division of Gastroenterology and Hepatology, Medical Department, Charité – Universitätsmedizin Berlin, Berlin, Germany
2 Berlin Institute of Health (BIH), Berlin, Germany
3 Berlin Institute for Medical Systems Biology (BIMSB), Berlin, Germany
4 Division of Gastroenterology, Infectiology and Rheumatology, Medical Department, Charité – Universitätsmedizin Berlin, Berlin, Germany
5 Department of Molecular Biology, Max Planck Institute for Infection Biology, Berlin, Germany
*Corresponding author. Tel.: +49-30-450-514-102; Fax: +49-30-450-514-923; E-mail: michael.sigal@charite.de

*et al*, 2017). The epithelium can be divided into the "gland base module" consisting of stem cells as well as gland base secretory cells (Tan *et al*, 2020), and the "pit module" consisting of surface mucous cells. The base module relies on stromal-derived Rspo3, which binds to Lgr receptors that associate with and prevent turnover of the Wnt/ Lrp/ Frizzled receptors complex, thereby stabilizing Wnt signaling (de Lau *et al*, 2011). Lgr4 is expressed broadly throughout the gland, while *Lgr5* is itself a target gene of Rspo3 signaling and is found exclusively in the base (Sigal *et al*, 2017). Loss of *Rspo3* results in a loss of the gland base module, while the increased *Rspo3* expression upon infection with *H. pylori* drives stem cell expansion and accumulation of gland base secretory cells. We have previously shown that Rspo3 counterbalances colonization and gland infiltration of *H. pylori* and mechanistically drives expansion of rapidly cycling Axin2 + /Lgr4 + /Lgr5- cells in the isthmus, as well as slowly cycling Axin2 + /Lgr4+/Lgr5 + basal cells that differentiate into secretory cells leading to hyperplasia in the antrum (Sigal *et al*, 2015, 2017, 2019). While this suggests that both Lgr4 and Lgr5 are likely to play a role in mediating the effects of Rspo, their distinct roles in driving antral pathobiology remain elusive.

Here, we applied conditional knockout mice that lack Lgr4 or Lgr5 to explore their involvement in antral mucosal responses to *H. pylori* infection. We reveal that Lgr4 expression is required to maintain expression of Lgr5 in the gland base. Depletion of Lgr4, but not Lgr5 alone, results in a diminished hyperplasia as well reduced inflammatory response, and we demonstrate that the Rspo-Lgr axis does not only promote hyperplasia but is also important for the ability of gland base cells to induce epithelial pro-inflammatory NF-κB signaling upon infection. Our data reveal an explanation for the unique ability of the stem cell compartment to respond to *H. pylori* infection and demonstrate a novel link between epithelial stem cells and innate immunity in the stomach.

# Results

### Lgr4/5, but not Lgr5 alone, is required for *Helicobacter pylori*-driven gland base cell expansion and hyperplasia

Lgr5 and Lgr4 are the Rspo receptors expressed in gastric epithelial cells. While *Lgr5* itself is a Wnt target gene, *Lgr4* is regulated

differently (Barker *et al*, 2007). Expression of *Lgr5* is thus limited to base cells, where Wnt/ Rspo concentrations are highest, while *Lgr4* is broadly expressed throughout the antral gland. *In situ* hybridization and analysis of publicly available single-cell RNA-seq data confirmed the broader expression of Lgr4 in the stomach, and we noticed the highest concentration of Lgr4 in the isthmus (Fig EV1A–C). Rspo3 triggers expansion of slower-cycling Lgr5+ base cells and rapid-cycling Lgr4+ isthmus cells, leading to hyperplasia in the antrum upon infection with *H. pylori*. Both cell types are considered progenitor cells that co-express the classic Wnt target gene Axin2 and are in direct contact with *H. pylori* micro-colonies (Sigal *et al*, 2015, 2017, 2019). To examine the specific roles of Lgr4 and Lgr5 under homeostatic conditions and upon infection with *H. pylori*, we generated conditional knockout (KO) mice, achieved by floxed sites, which enable a depletion of *Lgr5* or *Lgr4* (Planas-Paz *et al*, 2016) in Axin2 + stem cells upon injection of tamoxifen (B6-Axin2$^{CreErt2}$/Lgr5$^{fl/fl}$ and B6-Axin2$^{CreErt2}$/Lgr4$^{fl/fl}$, hereafter referred to as *Lgr5$^{-/-}$* and *Lgr4$^{-/-}$*), while B6-Axin2$^{CreErt2}$/Lgr5$^{+/+}$ and B6-Axin2$^{CreErt2}$/Lgr4$^{+/+}$ littermates served as controls. For experiments without infection, mice were treated with tamoxifen 14 days before sacrifice, allowing repopulation of glands by mutant cells. For infection experiments, some mice were infected 14 days after tamoxifen treatment with *H. pylori* and sacrificed 2 months later. All infected mice showed deep gland colonization (examples are shown in Fig EV2A). We first examined the effects of *Lgr5* depletion. Infection led to hyperplasia in both the control mice and in the *Lgr5$^{-/-}$* mice (Fig 1A and B). We earlier described that infection also leads to upregulation of *Lgr5* (Sigal *et al*, 2019). To visualize mucous gland base cells in the antrum, we used immunofluorescence labeling for lectin GSII (GSII) and gastric intrinsic factor (GIF). Only a subpopulation of GSII + cells were GIF positive (Figs 1A and EV2B). Proliferating isthmus cells were identified by anti-Ki67 staining and pit cells by anti-MUC5AC. In *Lgr5$^{-/-}$* mice, we did not detect changes in GSII + , GIF + , or Ki67+ cells, nor change in the morphology of the gland base. Upon infection, immunofluorescence showed an expansion of the GSII + GIF + compartment in both the control and the *Lgr5$^{-/-}$* mice. Hyperplastic glands in the *Lgr5$^{-/-}$* mice as well as in the littermate controls were populated by an increased number of Ki67+ cells (Fig 1A and C). We did not observe any significant alterations in *H. pylori* colony-forming units (CFUs) in *Lgr5$^{-/-}$* mice compared with control mice (Fig 1D). Gene expression analysis under homeostasis

---

**Figure 1.** Lgr5 is dispensable for gastric gland hyperplasia, gland base expansion, and antimicrobial defense upon infection with *Helicobacter pylori*.

*Lgr5$^{fl/fl}$/Axin2$^{CreErt2}$* (*Lgr5$^{-/-}$*) and control mice were infected for 2 months with *H. pylori*.

- A   Representative H&E staining from antral glands (upper row). The dotted line marks the gland base cell area, which expands upon infection in *Lgr5$^{-/-}$* and control mice. Immunofluorescence labeling for GSII and Ki67 (middle row) and GIF and Muc5ac (lower row) of antral epithelium from *Lgr5$^{-/-}$* and control mice uninfected and after 2 months of infection. Scale bars: 50 μm.
- B   Quantification of antral gland height in *Lgr5$^{-/-}$* compared with control mice. Uninfected control (n = 5) versus uninfected *Lgr5$^{-/-}$* (n = 4) versus infected control (n = 4) *versus* infected *Lgr5$^{-/-}$* (n = 4).
- C   Quantifications of GSII+ area (n = 4–5 biological replicates per group, n = 10 glands per mouse), Ki67 as percentage of total DAPI-stained cells (n = 3–4 biological replicates per group, n = 20 glands per mouse), GIF+ area (n = 4–5 biological replicates per group, n = 10 glands per mouse), Muc5ac + area (n = 4–5 biological replicates per group, n = 10 glands per mouse).
- D   *Helicobacter pylori* CFUs in *Lgr5$^{-/-}$* (n = 5) and control mice (n = 5).
- E   qPCR expression levels of *Lgr4*, *Lgr5*, and *Axin2*, gland base cell markers (*Gif*, *Pgc*, *Tff2*, and *Muc6*), pit cell marker *Muc5ac*, and *Itln1* in uninfected *Lgr5$^{-/-}$* (n = 6–10) and control mice (n = 4–10).
- F   qPCR expression levels of *Lgr4*, *Lgr5*, gland base cell markers (*Gif*, *Pgc*, and *Muc6*), and *Itln1* in *Lgr5$^{-/-}$* (n = 5) and control mice (n = 5) after 2 months of infection.

Data information: For (B, C, D, E, and F), data are mean + SD. *$P < 0.05$; **$P < 0.01$; ***$P < 0.001$; ns, not significant (one-way ANOVA + Tukey's multiple comparison test for B, C, *t*-test for D, E and F).
Source data are available online for this figure.
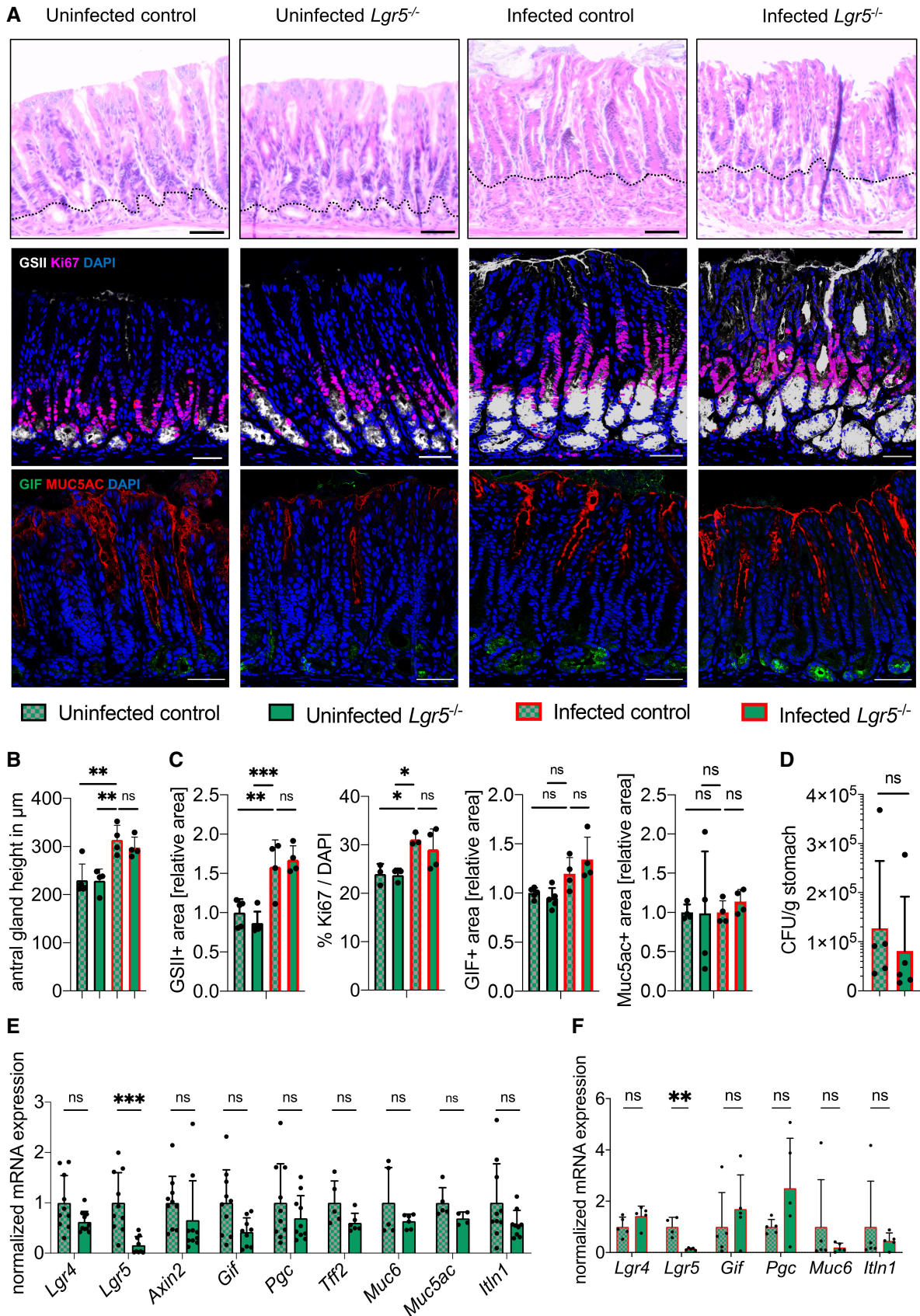
Figure 1.

and upon infection similarly revealed no significant changes in base cell markers (*Axin2, Gif, Pgc, Tff2,* and *Muc6*) or pit cell marker *Muc5ac* in control versus in *Lgr5*$^{-/-}$ mice (Fig 1E and F). Expression of *Itln1*, which we previously found to be expressed in gland base secretory cells and which binds *H. pylori* to counterbalance infection (Sigal *et al*, 2019), was also not significantly reduced. Although in an earlier study we showed that selective deletion of Lgr5-expressing cells leads to increased colonization with *H. pylori* (Sigal *et al*, 2019), the current data suggest that this phenomenon as well as the epithelial response to infection does not require Lgr5 expression.

We next explored the responses of *Lgr4*$^{-/-}$ mice to *H. pylori* and found that they failed to develop hyperplasia (Fig 2A and B). Immunofluorescence showed an expansion of both the Ki67+ and the GSII+GIF+ compartment in control, but not in *Lgr4*$^{-/-}$ mice (Fig 2A and C). *H. pylori* CFUs were significantly higher in Lgr4$^{-/-}$ compared with control mice (Fig 2D), mimicking the effects of *Rspo3* depletion that we described previously (Sigal *et al*, 2019). Notably, even in the absence of infection, gland bases of *Lgr4*$^{-/-}$ mice contained fewer GSII+ cells. A significant reduction in expression of *Lgr5, Axin2*, and *Gif* was detected in uninfected *Lgr4*$^{-/-}$ mice compared with uninfected control littermates (Fig 2E), which indicated that Lgr4 is required for *Lgr5* expression and Lgr5+ cell differentiation. Our finding that *Lgr4*$^{-/-}$ mice harbor fewer stem and secretory cells upon infection was further corroborated by gene expression analysis where we observed a significant decrease in expression of *Lgr5, Gif, Pgc,* and *Muc6* (Fig 2F). Both in homeostasis and in infection conditions, *Lgr4*$^{-/-}$ mice also expressed lower levels of *Itln1*, which is in accordance with the elevated *H. pylori* colonization levels observed. Thus, we conclude that Lgr4 expression represents a prerequisite for expression of Lgr5. While this makes it impossible to explore the role of Lgr4 alone, our data indicate that expression of Lgr4 is essential for gastric gland hyperplasia upon infection, gland base expansion, and antimicrobial defense upon *H. pylori* infection, while these parameters are unaffected upon loss of Lgr5 alone.

## R-spondin 3–Lgr signaling enables inflammatory responses to *H. pylori*

To obtain deeper insight into the effects of Lgr4 depletion in the stomach, we performed whole-transcriptome microarray analysis on whole antral tissue from 2-month *H. pylori*-infected *Lgr4*$^{-/-}$ mice and littermate controls. Gene set enrichment analysis (GSEA) confirmed that the loss of *Lgr4* (which, as shown above also leads to the loss of *Lgr5* expression) led to a reduction in the antral stem cell signature (Barker *et al*, 2010) and genes associated with beta-catenin signaling (Herbst *et al*, 2014) (Fig 3A and B). The downregulation of the Wnt target genes Axin2 and Sox9 was validated by qPCR (Fig 3C). In infected wildtype control, but not in infected Lgr4$^{-/-}$ mice, we identified nuclear beta-catenin (Ctnnb1) in Ki67+ and GSII+ cells in the gland (Fig EV2C). Intriguingly, we found that various inflammation-associated genes were differentially expressed in control versus *Lgr4*$^{-/-}$ mice and GO enrichment analysis further revealed that 63 out of the 157 downregulated genes were linked to innate immune signaling via NF-κB and to TNF-α signaling via NF-κB (Table EV1, Fig 3D).

We analyzed by immunofluorescence the key NF-κB subunit mediating innate immune response p65 as well as p65 acetyl K310 (Fig 3E–G). Acetylation of p65 at lysine 310 on p65 is required for full transcriptional activation of NF-κB (Chen *et al*, 2002). Total p65 localized predominantly in the lower Ki67+ gland isthmus compartment in uninfected mice. In infected control mice, p65 level was increased in the expanded Ki67+ compartment and at less intensity in the GSII+ cells. In contrast, p65 level was not increased in *H. pylori*-infected *Lgr4*$^{-/-}$ mice (Fig 3E and F). Inhibition of *H. pylori*-induced NF-κB signaling by deletion of Lgr4 became obvious by staining for the activated p65 (p65 at K310), which revealed a strong expression exclusively in the glands of infected control, but not of infected *Lgr4*$^{-/-}$ mice (Fig 3G).

To corroborate this revelation, we tested for expression of NF-κB target genes in uninfected and infected *Lgr4*$^{-/-}$ mice and controls by qPCR. Expressions of *Cxcl1* and *Cxcl2*, considered murine homologs of *IL-8*, as well as Cxcl10 and Ccl2, both prominently regulated in the microarray data (Table EV1), were upregulated upon infection only in control, but not in Lgr4$^{-/-}$ mice (Fig 3H). Immunofluorescence for Cxcl1 further confirmed activation of NF-κB signaling in the lower gland isthmus proliferative cell compartment (Fig 3I). Taken together, our *in vivo* experiments reveal that Lgr4 is required for NF-κB activation and expression of pro-inflammatory chemokines in response to *H. pylori* infection.

---

**Figure 2. Lgr4 regulates hyperplasia and expansion of gland base cells upon infection with *Helicobacter pylori*.**

*Lgr4*$^{fl/fl}$/*Axin2*$^{CreErt2}$ (*Lgr4*$^{-/-}$) and control mice were infected for 2 months with *H. pylori*.

A   Representative H&E staining from antral glands (upper row). The dotted line marks the gland base cell area, which does not expand in infected *Lgr4*$^{-/-}$ but does expand in the corresponding control mice. Immunofluorescence labeling for GSII and Ki67 (middle row) and GIF and Muc5ac (bottom row) of antral epithelium from *Lgr4*$^{-/-}$ and control mice uninfected and after 2 months of infection. Scale bars: 50 μm.

B   Quantification of antral gland height in *Lgr4*$^{-/-}$ compared with control mice. Uninfected control (*n* = 2) versus uninfected *Lgr4*$^{-/-}$ (*n* = 4) versus infected control (*n* = 4) versus infected *Lgr4*$^{-/-}$ (*n* = 4).

C   Quantifications of GSII+ area (*n* = 2–4 biological replicates per group, *n* = 10 glands per mouse), Ki67 as percentage of total DAPI-stained cells (*n* = 2–4 biological replicates per group, *n* = 20 glands per mouse), GIF+ area (*n* = 2–4 biological replicates per group, *n* = 10 glands per mouse), Muc5ac + area (*n* = 4–5 biological replicates per group, *n* = 10 glands per mouse).

D   *Helicobacter pylori* CFUs show higher colonization in *Lgr4*$^{-/-}$ (*n* = 5) compared with control mice (*n* = 4).

E   qPCR expression levels of *Lgr4, Lgr5, Axin2*, gland base cell markers (*Gif, Pgc, Tff2,* and *Muc6*), pit cell marker *Muc5ac*, and *Itln1* in uninfected *Lgr4*$^{-/-}$ (*n* = 4–10) and control mice (*n* = 4–6).

F   qPCR expression levels of *Lgr4, Lgr5*, gland base cell markers (*Gif, Pgc,* and *Muc6*), and *Itln1* in *Lgr4*$^{-/-}$ (*n* = 5) and control mice (*n* = 5) after 2 months of infection.

Data information: For (B, C, D, E, and F), data are mean + SD. *P < 0.05; **P < 0.01; ***P < 0.001; ****P < 0.0001; ns, not significant (one-way ANOVA + Tukey's multiple comparison test for B, C, *t*-test for D, E, and F).

Source data are available online for this figure.
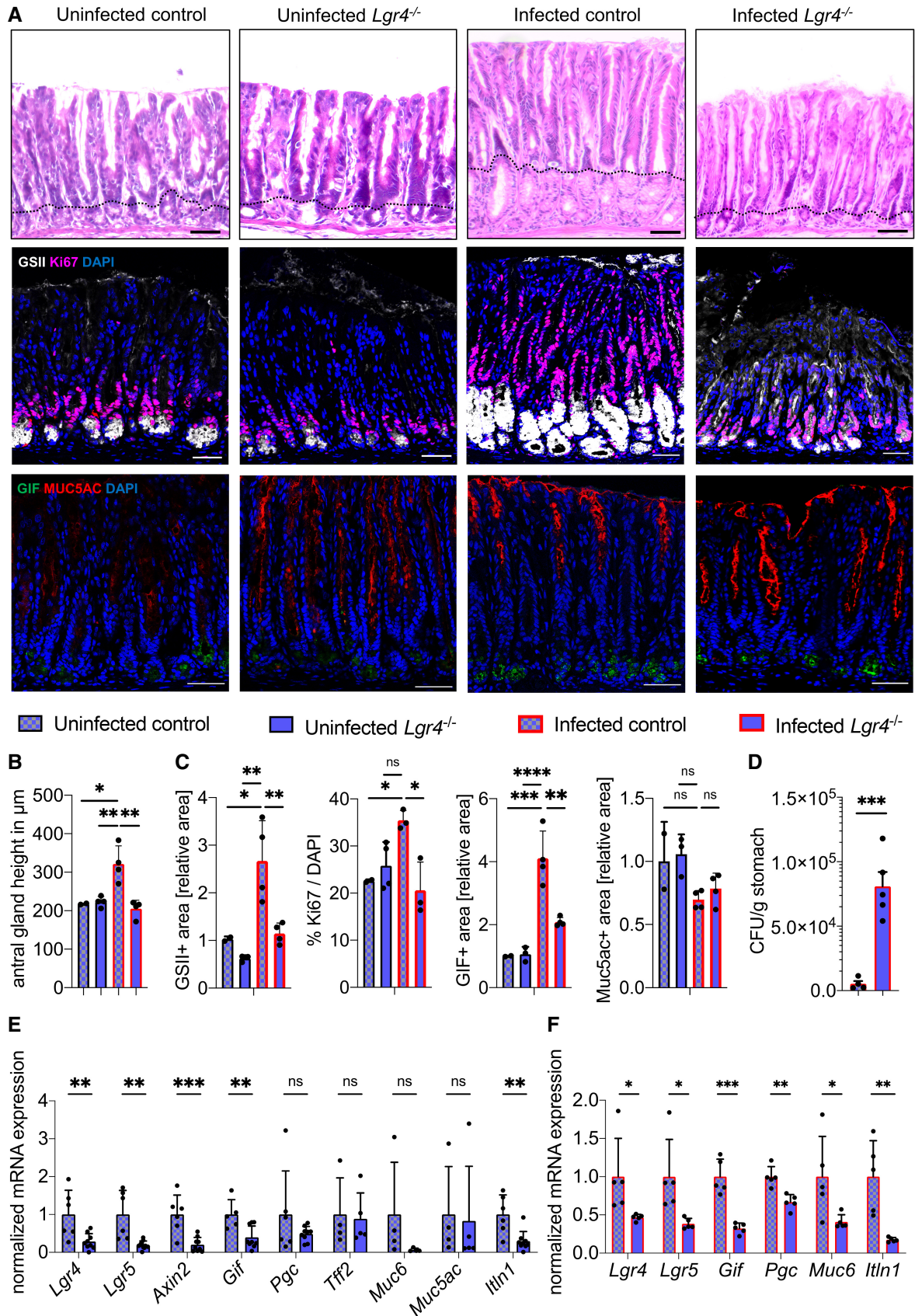
**Figure 2.**
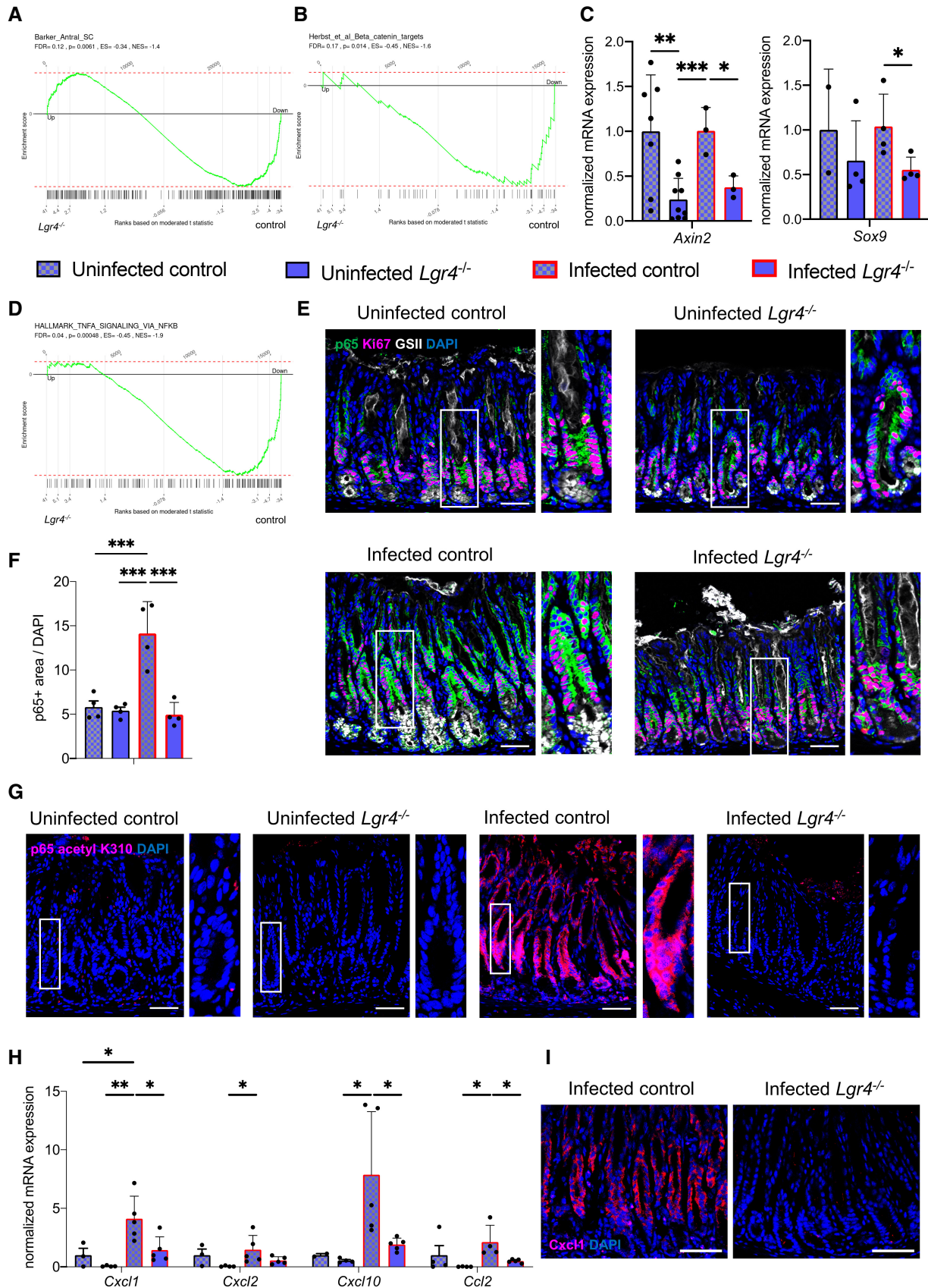
**Figure 3.**

**Figure 3. Lgr4 regulates stem cells and NF-κB signaling in the antrum.**

A, B  GSEA comparing microarray data from 2-month-infected *Lgr4*<sup>fl/fl</sup>/*Axin2*<sup>CreErt2</sup> (*Lgr4*<sup>−/−</sup>) mice with publicly available data demonstrating downregulation of antral stem cell signature (A) and beta-catenin targets (B).

C  qPCR expression levels for beta-catenin targets *Axin2* and *Sox9* in uninfected and infected *Lgr4*<sup>−/−</sup> and control mice (*n* = 2–9).

D  GSEA comparing microarray data from 2-month-infected *Lgr4*<sup>−/−</sup> mice with publicly available data demonstrating downregulation of the TNF-α signaling via NF-κB.

E  Immunofluorescence labeling for p65, Ki67, and GSII in the mouse antrum tissue from uninfected and infected *Lgr4*<sup>−/−</sup> and control mice. Insets show magnified images. Scale bars: 50 μm.

F  Quantification of p65+ area as percentage of total DAPI-stained cells of uninfected and infected *Lgr4*<sup>−/−</sup> and control mice (*n* = 4 biological replicates per group, *n* = 20 glands per mouse).

G  Immunofluorescence co-localization of p65 acetyl K310 (activated form of NF-κB) in the mouse antrum tissue of infected *Lgr4*<sup>−/−</sup> and in control mice. Insets show magnified images. Scale bars: 50 μm.

H  qPCR expression levels of *Cxcl1*, *Cxcl2*, *Cxcl10*, and *Ccl2* in uninfected and infected *Lgr4*<sup>−/−</sup> mice (*n* = 4–5) and control mice (*n* = 2–5).

I  Immunofluorescence labeling for Cxcl1 in the mouse antrum tissue in infected *Lgr4*<sup>−/−</sup> and in control mice. Scale bars: 50 μm.

Data information: For (G and I) images represent findings that were reproduced at least twice in the laboratory in independent biological replicates. For (C, F, and H), data are mean + SD. *$P < 0.05$; **$P < 0.01$; ***$P < 0.001$ (one-way ANOVA + Tukey's multiple comparison test).
Source data are available online for this figure.

---

To validate that these effects are directly related to the Rspo3-Lgr regulatory axis, we analyzed NF-κB expression and target genes in tamoxifen-treated, 2-week- or 2-month-infected B6-*Myh11*<sup>CreErt2</sup>/*Rspondin3*<sup>fl/fl</sup> mice (here referred to as: *Rspo3*<sup>−/−</sup>), in which *Rspo3* is knocked out specifically in myofibroblasts beneath the gland base, as described previously (Sigal *et al*, 2019). B6-*Myh11*<sup>CreErt2</sup>/*Rspondin3*<sup>+/+</sup> littermates served as controls. In 2-week-infected control mice, we observed a strong expression of p65 specifically in the gland isthmus with a pronounced nuclear translocation of p65, while *Rspo3* KO led to reduced expression of p65 (Fig 4A and B). In contrast, cells in the pit and surface region of both *Rspo3*<sup>−/−</sup> and control mice were almost completely devoid of p65 protein, despite the infection. *Rspo3* KO also led to reduced expression of *Cxcl1* and *Cxcl2* at 2 weeks and 2 months of infection, as determined by qPCR (Fig 4C and D). We also generated mice to conditionally overexpress *Rspo3* in Myh11+ mesenchymal cells (*Myh11*<sup>CreERT2</sup>/*Rosa26Sor*<sup>6(CAG-Rspo3)</sup>, here referred to as: *Rspo3* KI) and found that infection in these mice leads to a strong upregulation of p65, GSII and Ki67 compared with infected control mice (Fig 4E–H). Notably, *Rspo3* KI upregulated p65 also in uninfected mice in the antrum as well as in the colon (Figs 4F and EV3A). The massive hyperplastic glands in *Rspo3* KI mice revealed throughout the epithelium intense signals for nuclear p65 acetyl K310 (Fig 4I). Collectively, our results reveal that the Rspo3-Lgr axis not only induces Wnt but also enables an activation of NF-κB signaling baseline and upon infection, facilitating the induction of epithelial pro-inflammatory chemokines in response to bacteria *in vivo*.

**R-spondin 3–Lgr4–NF-κB signaling is responsible for neutrophil infiltration in *H. pylori* gastritis**

In *H. pylori*-infected mice, we observed a manifestation of proinflammatory processes, including neutrophil chemotaxis and immune response in dependence of *Lgr4*, by separately examining genes that are experimentally validated as targets of NF-κB (see https://www.bu.edu/nf-kb/gene-resources/target-genes/) and whose expression was decreased in *Lgr4*<sup>−/−</sup> mice (Fig EV3B). We, therefore, asked if infiltration of immune cells upon infection is dependent on Lgr4 or Lgr5. Using immunofluorescence, we stained for MPO, IBA1, and CD3 to analyze the presence of neutrophils, macrophages, and T cells, respectively, in *Lgr4*<sup>−/−</sup> mice in uninfected and infected conditions as well as in control mice. As expected, infection led to high mucosal influx of all analyzed immune cells, predominantly in the proximal antrum. Interestingly in infected *Lgr4*<sup>−/−</sup> mice, neutrophil infiltration was significantly diminished, indicating that a lack of proper epithelial Lgr signaling has a functional consequence with regard to the recruitment of inflammatory cells (Fig 5A and B). Recruitment of macrophages and T cells was not

---

**Figure 4. Rspo promotes accumulation of nuclear p65.**

A  Immunofluorescence labeling for p65 and E-cadherin in the mouse antrum tissue of 2-week-infected B6-*Myh11*<sup>CreErt2</sup>/*Rspondin3*<sup>fl/fl</sup> (*Rspo3*<sup>−/−</sup>) and control mice. Arrows in infected control mice indicate nuclear p65 that is not observed in *Rspo3*<sup>−/−</sup> mice. Scale bars: 50 μm.

B  Quantification of p65+ area as percentage of total DAPI-stained cells of infected *Rspo3*<sup>−/−</sup> and control mice (*n* = 3 biological replicates per group, *n* = 20 glands per mouse).

C  qPCR expression level of *Cxcl1* and *Cxcl2* in 2-week-infected *Rspo3*<sup>−/−</sup> mice (*n* = 3) versus infected control mice (*n* = 4).

D  qPCR expression level of *Cxcl1* and *Cxcl2* in 2-month-infected *Rspo3*<sup>−/−</sup> mice (*n* = 5) versus infected control mice (*n* = 6).

E  *Myh11*<sup>CreERT2</sup>/*Rosa26Sor*<sup>6(CAG-Rspo3)</sup> (*Rspo3* KI) mice were infected for 6 weeks with *H. pylori*. Immunofluorescence labeling for p65, GSII and KI67 in uninfected and infected *Rspo3* KI and control mice. Scale bars: 50 μm.

F  Quantification of p65+ area as percentage of total DAPI-stained cells of uninfected and infected *Rspo3* KI and control mice (*n* = 2–3 biological replicates per group, *n* = 20 glands per mouse).

G  Quantification of GSII+ area of uninfected and infected *Rspo3* KI and control mice (*n* = 2–3 biological replicates per group, *n* = 20 glands per mouse).

H  Quantification of Ki67 as percentage of total DAPI-stained cells of uninfected and infected *Rspo3* KI and control mice (*n* = 2–3 biological replicates per group, *n* = 20 glands per mouse).

I  Immunofluorescence labeling for p65 acetyl K310 in infected *Rspo3* KI and control mice. Insets show magnified images. Scale bars: 50 μm.

Data information: For (B, C, D, F, G, and H) data are mean + SD. *$P < 0.05$; **$P < 0.01$; ns, not significant (*t*-test for B, C, and D, one-way ANOVA + Tukey's multiple comparison test for F, G and H).
Source data are available online for this figure.
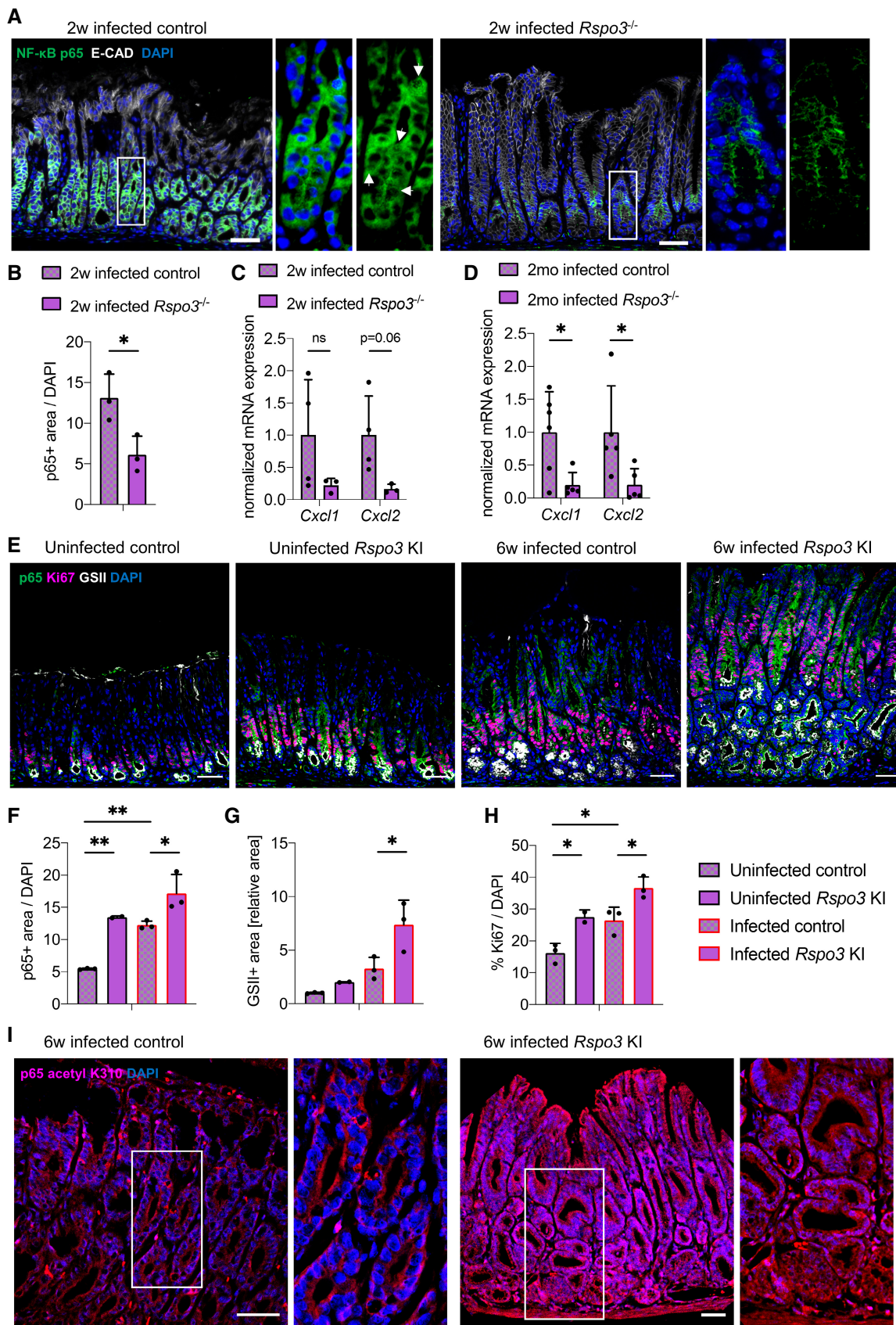
Figure 4.
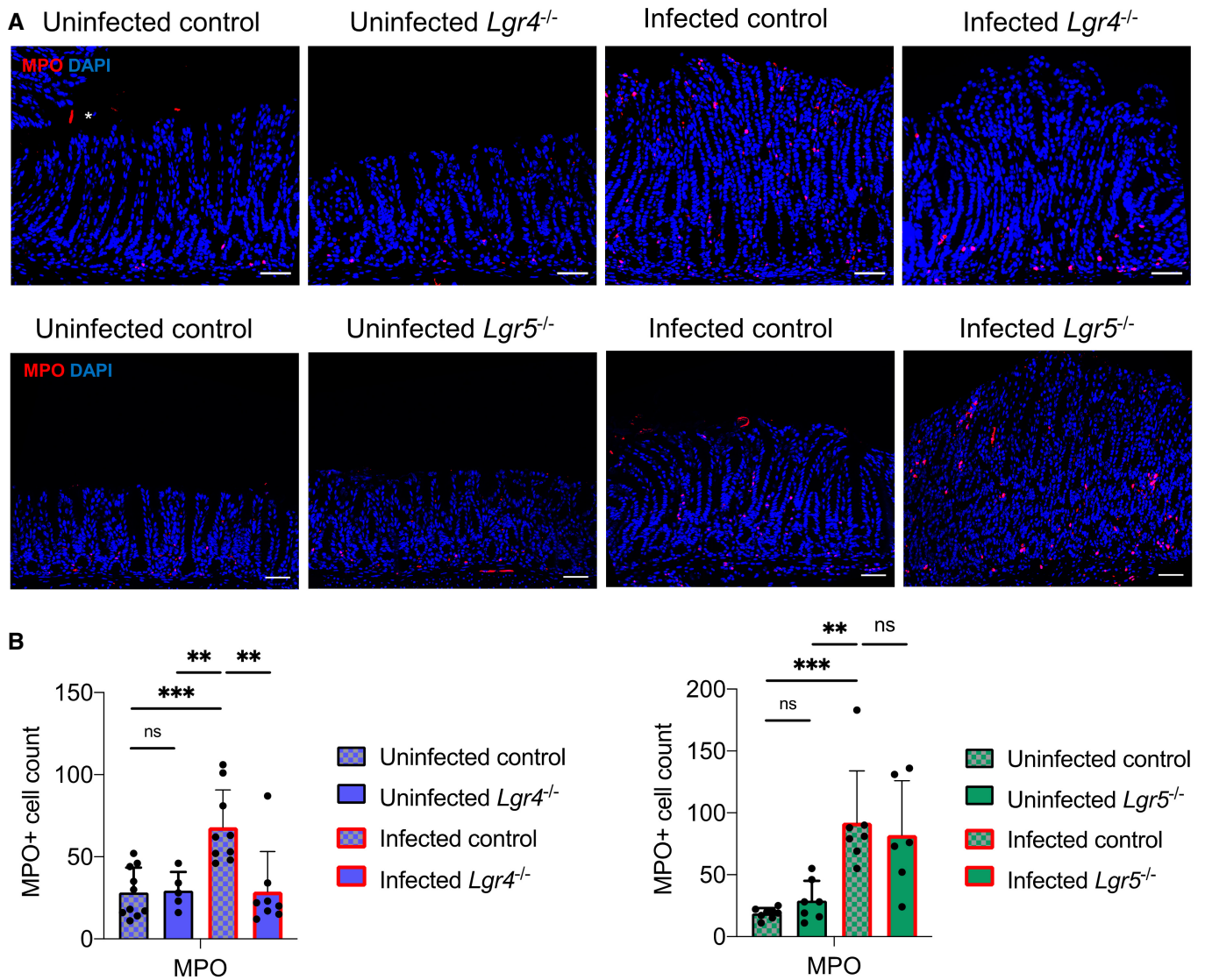
**Figure 5. Lgr4 controls mucosal neutrophil infiltration.**

A  Immunofluorescence labeling for MPO in uninfected and 2-month-infected *Lgr4*$^{-/-}$ and control mice (top panel) and 2-month-infected *Lgr5*$^{-/-}$ and control mice (bottom panel). Asterisks indicate nonspecific staining. Scale bars: 50 μm.

B  Quantification of MPO+ cells in uninfected and 2-month-infected *Lgr4*$^{-/-}$ and control mice (n = 2 biological replicates per group, n = 5–10 FOVs per mouse) (left panel) and 2-month-infected *Lgr5*$^{-/-}$ and control mice (n = 2 biological replicates per group, n = 6–8 FOVs per mouse) (right panel).

Data information: For (B) data are mean + SD. **$P < 0.01$; ***$P < 0.001$; ns, not significant (one-way ANOVA + Tukey's multiple comparison test).
Source data are available online for this figure.

significantly altered in these mice, which is in line with our similar observations in *Rspo3* KO mice (Sigal *et al*, 2019) and may point toward a distinct immune cell infiltration pattern with various influence factors in gastritis that warrants further investigation (Fig EV4A and B). Equivalent analysis of infected *Lgr5*$^{-/-}$ mice failed to detect altered immune cell infiltration (Figs 5A and B, and EV4A and B).

**Stem cells are the primary epithelial sensors of ADP heptose and promote pro-inflammatory signaling**

To discriminate between effects by immune cells and direct epithelial responses, we took advantage of the epithelial gastric organoid cultures. Gastric organoids were grown in the standard full medium (FM) containing Rspo and Wnt, which resembles the gland base environment and drives stem cell turnover. To test whether these growth factors affect the epithelial ability to mediate pro-inflammatory responses, some organoids were cultured in medium without Rspo, without Wnt and Rspo, or with the addition of Bmp2, which rapidly induces pit cell differentiation. Organoids grown in FM showed robust growth, while removal of growth factors or addition of Bmp2 led to reduced growth and a more spherical appearance (Fig 6A). Immunofluorescence analysis revealed that organoids grown in FM formed small invaginations, which corresponded to GSII+ gland base cells. As expected, upon removal of

Figure 6.

**Figure 6. Stem cells are the primary epithelial sensors of ADP heptose and promote pro-inflammatory signaling.**

Antrum organoids from wildtype mice were grown in full medium (FM) for 2–3 days, followed by respective medium conditions for 3–5 days (FM, −Rspo, −Rspo/-Wnt, +BMP2). 0.5 µM ADP heptose or 10 ng/ml TNF-α was added for 2 h to all organoid conditions prior to analysis.

A  Bright-field images of organoids in respective conditions before treatment with ADP heptose or TNF-α. Scale bars: 200 µm.
B  Immunofluorescence labeling for GSII and Muc5ac of organoids in respective conditions before treatment with ADP heptose or TNF-α. Scale bars: 50 µm.
C  qPCR expression level of *Lgr5* in untreated organoids in respective medium conditions (*n* = 4–5 biological replicates).
D  qPCR expression level of *Gif* in untreated organoids in respective medium conditions (*n* = 4–5 biological replicates).
E  qPCR expression level of *Cxcl1*, *Cxcl2*, *Cxcl10*, and *Ccl2* in organoids after treatment with ADP heptose compared with untreated controls within the respective medium conditions (*n* = 6 biological replicates per condition).
F  qPCR expression level of *Cxcl1*, *Cxcl2*, *Cxcl10*, and *Ccl2* in organoids after treatment with TNF-α compared with untreated controls within the respective medium conditions (*n* = 2–3 biological replicates per condition).

Data information: For (C, D, E, and F) data are mean + SD. *$P < 0.05$; **$P < 0.01$; ****$P < 0.0001$ (one-way ANOVA + Tukey's multiple comparison test for C and D; *t*-test for E and F). Genes without asterisks are not significantly altered.
Source data are available online for this figure.

growth factors, invaginations and GSII + cells were lost, while more MUC5AC + pit cells were detected (Fig 6B). Expression of the stem cell marker Lgr5, as well as the gland base mucous cell marker Gif, was strongly downregulated in all other conditions compared with stem cell-enriched organoids (FM), as analyzed by qPCR (Fig 6C and D).

To investigate the mechanism by which NF-κB could be induced upon *H. pylori* infection, we treated gastric organoids with ADP heptose, a bacterial sugar, which was previously shown to induce NF-κB in the context of *H. pylori* infection (Pfannkuch *et al*, 2019). We thus exposed organoids grown in the different medium conditions to ADP heptose for 2 h, to examine their ability to activate NF-κB. The inflammatory response was measured via qPCR of Cxcl1 and Cxcl2, which are classic murine ADP heptose readouts (Brooks *et al*, 2020) as well as *Ccl2* and *Cxcl10*, which we found to be upregulated in an Rspo3/Lgr4-dependent manner after *H. pylori* infection *in vivo*. ADP heptose triggered NF-κB target gene expression in organoids grown in FM, while organoids grown in the absence of Rspo and Wnt signaling remained unresponsive (Fig 6E). Notably, the absence of Rspo alone already prevented full activation of NF-κB signaling, demonstrating the critical role of Rspo signaling for maintaining the ability of the cells to induce epithelial pro-inflammatory signaling. To address whether these responses are limited to ADP heptose or also affect other pro-inflammatory pathways, we treated organoids with TNF-α. We found similar effects of growth factor withdrawal, indicating that NF-κB activation in gland base cells is not limited to ADP heptose-induced signaling and that activation via the classical TNF-α pathway also depends on Rspo signaling (Fig 6F).

To determine whether this phenotype is indeed due to the activation of NF-κB, we quantitated DNA binding activity of the transcription factor by electrophoretic mobility shift assay (EMSA) in organoids treated as above (Fig 7A and B). We observed baseline activity of NF-κB in dependence of Rspo and demonstrated that the presence of Rspo is necessary for the pronounced induced activation of NF-κB and of its upstream kinase, IKK (IκB kinase). Removal of Rspo or Wnt led to a partial loss of a *bona fide* target of NF-κB, IκBα (*Nfkbia*). Supershift analysis in FM organoids + ADP heptose with antibodies against the five subunits confirmed p65 as the principal mediator (Fig 7C). These findings confirm that induction of the canonical IKK-NF-κB pathway in response to ADP heptose in gastric epithelium requires functional Wnt/ Rspo signaling.

To determine which cells in ADP heptose-treated organoids harbor nuclear p65, we stained organoids treated as above with antibodies against total p65 and Ki67 or GSII (Fig EV5A). Nuclear translocation of p65 was detected in nuclei of Ki67 + and GSII + cells in organoids in FM treated with ADP heptose. We confirmed our findings by generating gastric organoids from a NF-κB reporter mouse line, κ-EGFP (Brischetto *et al*, 2021). In epithelium, activated NF-κB localized to Ki67 + and partially to GSII + cells and was nearly absent in organoids without Rspo or Wnt or in organoids treated with Bmp2. In the latter conditions, NF-κB activity was not observed upon ADP heptose treatment, indicating that Rspo/Wnt are necessary for an activation of NF-κB (Fig EV5B and C). Taken together, we find that NF-κB activation and subsequent chemokine expression occurs in epithelial gland base cells in an Rspo-dependent manner.

## NF-κB signaling is important for gland base secretory cell differentiation

As we found that hyperplasia is triggered by Rspo3-Lgr signaling via base cell and isthmus cell expansion, we asked whether activated NF-κB, which is predominantly present in isthmus cells, contributes to the maintenance of one of these cell types. Therefore, we obtained mice with ubiquitously suppressed *NF-κB* activity, by using a transdominant negative mutant of IkBa (IkBaΔN) that was inserted in-frame into the beta-catenin locus (cI kappa B alpha Delta N, hereafter referred to as *ΔN*). Importantly, the beta-catenin protein expression and activity in these mice is not impaired (Schmidt-Ullrich *et al*, 2001). Strikingly, qPCR on antral organoids (Fig 8A) derived from these mice revealed not only reduced expression of NF-κB target genes, but also a strong reduction in the expression of gland base cell markers (Fig 8B and C), indicating that NF-κB activity is not only important for promoting inflammation but is in fact an integral factor determining gland base cell identity. Notably, *Lgr4* was higher in *ΔN* organoids, pointing to a compensatory mechanism upon base cell loss, which is not sufficient to maintain their identity (Fig 8B). Analysis of gastric tissue sections from *ΔN* mice showed that there was also a significant reduction in the number of GSII + secretory gland base cells *in vivo*, but not of proliferating cells (Fig 8D and E). We conclude that *NF-κB* signaling in the stem cell compartment is important for shifting cell differentiation in the base toward secretory cells, which could be an explanation for their accumulation upon *H. pylori* infection.
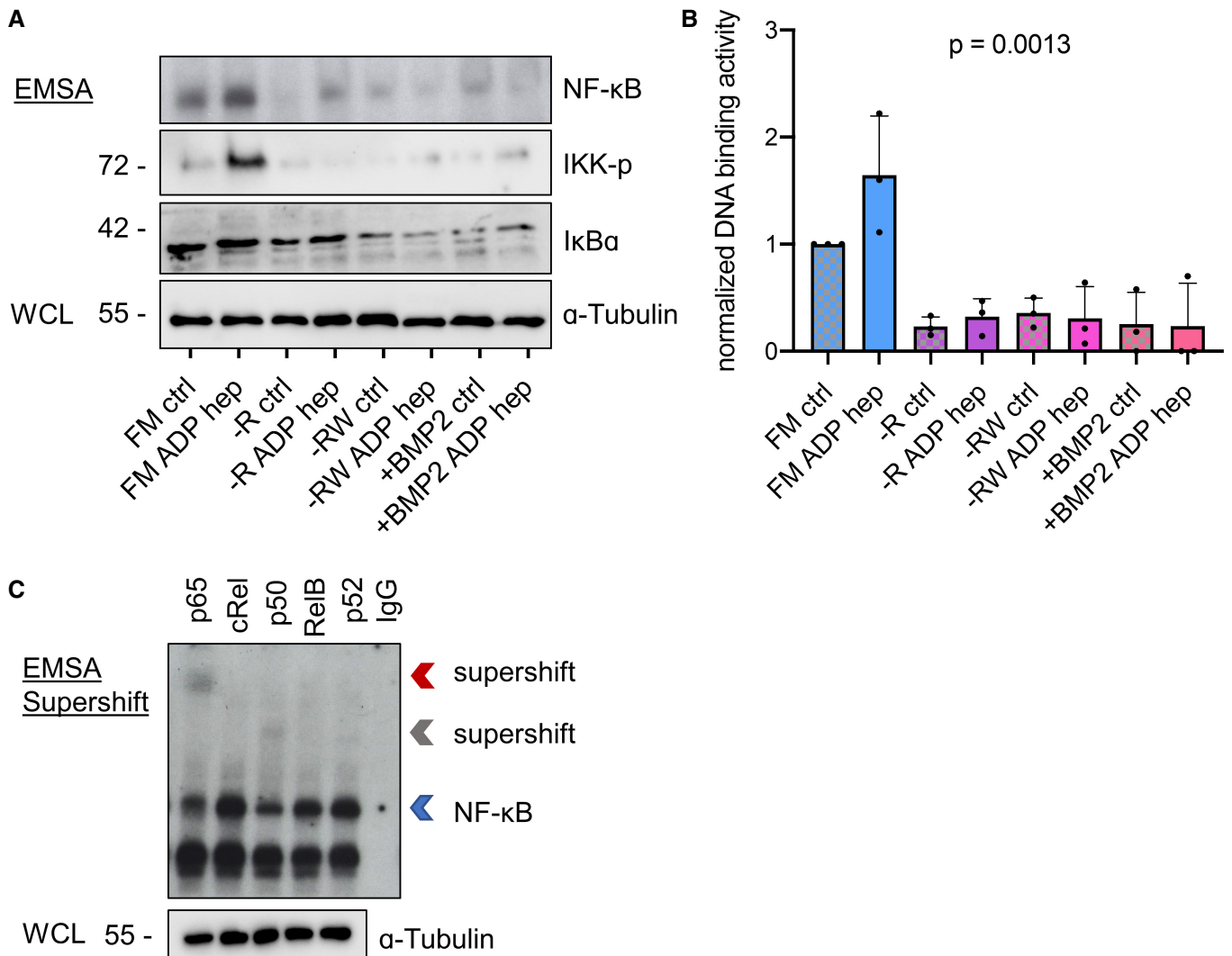
**Figure 7. Activation of IKK–NF-κB pathway by ADP heptose requires Wnt and Rspo.**

Antrum organoids from wildtype mice were grown in full medium (FM) for 2–3 days, followed by respective medium conditions for 3–5 days (FM, −Rspo, −Rspo/-Wnt, +BMP2). 0.5 µM ADP heptose was added for 2 h to all organoid conditions prior to analysis.

A   Electrophoretic mobility shift assay (EMSA) and SDS–PAGE western blot from whole-cell protein (WCL) lysates from gastric organoids untreated or treated with ADP heptose, and maintained either in FM in medium without Rspo, without Wnt and Rspo, or + BMP2. Representative images from $n$ = 3 biological replicates.

B   Quantification of EMSA based on $n$ = 3 biological replicates using ImageJ with normalization to loading (α-Tubulin).

C   EMSA supershift from FM + ADP heptose organoids with the antibodies indicated. Blue arrow indicates NF-κB binding. Red arrow points to gel expected locations of supershifts from antibodies against p65, cRel, or RelB. Gray arrow points to supershift location on the gel from antibodies against p52 or p50. IgG lane serves as a negative control.

Data information: For (B) data are mean + SD. Significance is calculated by one-way ANOVA, $F$ = 9.21.
Source data are available online for this figure.

# Discussion

Here, we demonstrate that the stem cell compartment in the stomach antrum is uniquely equipped to respond to infection and initiate mucosal inflammation. Our data reveal a link between Rspo-Lgr signaling and NF-κB, which enables the gland base compartment to rapidly initiate a pro-inflammatory response and simultaneously structurally adapt to *H. pylori* infection.

Most investigations of epithelial homeostasis that explore Rspo-Wnt signaling axis put a focus on Lgr5, which was originally

identified as a marker of intestinal and later of gastric stem cells (Barker *et al*, 2007, 2010). Lgr5 is a Wnt target gene that requires high levels of Wnt signaling (Segditsas *et al*, 2008). Such high Wnt activity depends *in vivo* in the stomach on the Wnt signaling enhancer Rspo3 produced by stromal myofibroblasts (Sigal *et al*, 2017; Harnack *et al*, 2019). Rspo molecules bind to Lgr4 and Lgr5 and prevent turnover of the Wnt receptor Frizzled (de Lau *et al*, 2011). Thus, Rspo signaling itself drives expression of its own receptor *Lgr5*, implying that a positive autocrine feedback loop that stabilizes Wnt/ Rspo signaling could exist (Yan *et al*, 2017). In

contrast, unlike Lgr5, Lgr4 is not a Wnt target gene and broadly expressed in the epithelium of the gastrointestinal tract, including the stomach (Sigal *et al*, 2017; Harnack *et al*, 2019). It has been shown that Lgr5 and Lgr4 act in concert to maintain homeostasis in the intestine (de Lau *et al*, 2011). While loss of Lgr5 + cells does not impact epithelial homeostasis and injury repair (Tian *et al*, 2011; Castillo-Azofeifa *et al*, 2019), loss of Lgr4, similar to loss of Rspo3, renders the epithelium more susceptible to injury (Liu *et al*, 2013; Greicius *et al*, 2018; Harnack *et al*, 2019). Depletion of Lgr5 + cells is followed by their recovery in the intestine and stomach, and this process has been shown to require Rspo3, which is likely through

interaction with Lgr4 (Sigal *et al*, 2017; Harnack *et al*, 2019). Our data here demonstrate that Lgr4 represents a critical receptor for mucosal responses to *H. pylori* in the antrum. Lgr4 also controls Lgr5 expression; however, Lgr5 alone does not impact *H. pylori* infection, indicating that while Lgr5 + cells are critical in the context of infection, their maintenance and function is not driven by Lgr5 alone, but requires Lgr4 expression. Therefore, the Rspo-Lgr4 axis is highly relevant for epithelial responses, while Lgr5 expression is a marker of Rspo signaling, but is largely dispensable for Rspo effects.

*Helicobacter pylori* colonizes the stomach of about 50% of the world's population and is the main risk factor for gastric cancer
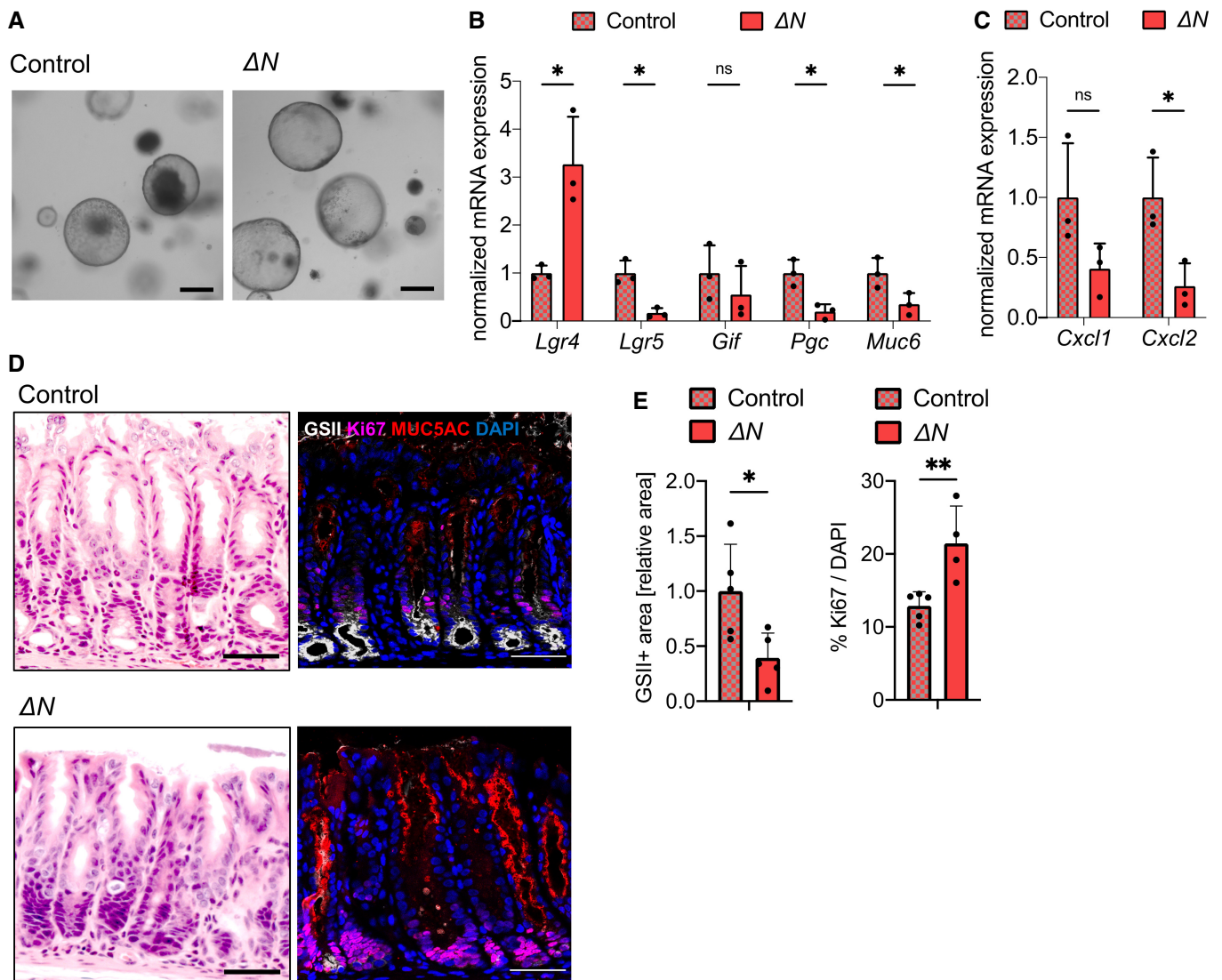


**Figure 8.  NF-κB activity defines gland base compartment in the antrum.**

A    Bright-field images of antrum organoids from *129;129P2-ctnnb1^tm(NFKBIAΔN)1Rsu* (*ΔN*) mice and control mice, passage 0, day 6. Scale bars: 500 μm.

B, C    qPCR expression levels of *Lgr4, Lgr5, Gif, Pgc, Muc6* (B) and *Cxcl1, Cxcl2* (C) of organoids (*n* = 3 biological replicates).

D    Representative H&E staining and immunofluorescence labeling for GSII, Ki67 and MUC5AC in uninfected *ΔN* and control mice. Scale bars: 50 μm.

E    Quantification of GSII and Ki67 as percentage of total DAPI-stained cells in *ΔN* and control mice (*n* = 5 biological replicates per group, *n* = 20 glands per mouse).

Data information: For (B, C, and E) data are mean + SD. *$P < 0.05$; **$P < 0.01$; ns, not significant (*t*-test).
Source data are available online for this figure.

(Parsonnet et al, 1997). Infection causes a chronic active gastritis, characterized by mucosal infiltration of immune cells such as neutrophils (Eck et al, 2000), which can progress to atrophic or hyperplastic gastritis, metaplasia and, in about 1% of patients, gastric cancer (Correa, 1995). Neutrophils are associated with mucosal damage in H. pylori gastritis (Ernst et al, 1997; Shimoyama & Crabtree, 1998). It is well established that the inflammatory response to infection is linked to epithelial pathology and mouse experiments have demonstrated that the degree of immune responses against H. pylori correlates with the degree of epithelial premalignant pathology, while the degree of inflammation correlates negatively with H. pylori colonization (Wunder et al, 2006; Arnold et al, 2011). The link between infection, inflammation, and epithelial pathology is not fully resolved. We have previously observed that colonization of gastric glands (in contrast to colonization of the surface pits) triggers inflammation, gland hyperplasia as well as metaplasia (Sigal et al, 2015). These responses result in an accumulation of antimicrobial gland base secretory cells, which limit gland colonization but fail to clear the infection (Sigal et al, 2019). Here, we demonstrate and mechanistically resolve the unique ability of the epithelial gland base module to initiate a pro-inflammatory NF-κB response that promotes an accumulation of gland base cells and simultaneously induces an upregulation of epithelial chemokines leading to mucosal neutrophil infiltration that can initiate and maintain a chronic active gastritis. These data provide an explanation for selective pro-inflammatory responses to gland-associated bacteria and link epithelial and inflammatory responses observed upon infection.

It is likely that this unique ability of gland and crypt base cells is not restricted to H. pylori infection in the stomach. Glands and crypts show a similar organization throughout the gastrointestinal tract, with stem cells located in the base. It will be interesting to investigate mechanisms of Rspo-NF-κB interactions in response to intestinal pathogens. While crypt colonization may be the most beneficial niche for chronic bacterial colonization as it may provide nutritional and physical benefits for colonization (Keilberg et al, 2016), bacterial penetration into this protected compartment that harbors stem cells is likely highly detrimental for the host. Indeed, several pathogens have evolved to target this compartment. In the colon Shigella flexneri reach the bottom of crypts to target stem cells leading to long-term repercussions for tissue regeneration (Arena et al, 2015). Moreover, Vibrio cholerae in the small intestine and Campylobacter jejuni in the cecum establish crypt colonization by directed and efficient swimming. Vibrio cholerae infect intestinal progenitor cells with a type VI secretion system blocking growth and repair pathways in addition to extensive tissue damage upon infection (Fast et al, 2020). Sensing of bacteria and the ability to initiate inflammation upon gland base cell colonization is, therefore, likely to be a conserved property of gland and crypt base cells, enabling a rapid response to these undesired events.

Progenitor cells in the gland are, therefore, not only responsible for gland repopulation but also play a key role in mucosal immunity. Modulation of gastrointestinal stem cell behavior by immune-derived signals has been shown previously. Stem cells in the small intestine express NOD2 receptors, and microbiota-derived peptidoglycans that activate NOD2 support stem cell survival (Nigro et al, 2014). T cell-derived cytokines have also been shown to modulate crypt differentiation, enabling epithelial adaptation to infectious stimuli (Biton et al, 2018). Here, we demonstrate that antral base cells not only respond to immune signals but act as critical components of the innate immune system by initiating responses to pathogenic bacteria via NF-κB signaling.

Molecular links between NF-κB and Wnt signaling in carcinogenesis have been established using genetic cancer models (Greten & Grivennikov, 2019), for example, in Wnt-induced intestinal cancer, enhanced NF-κB activity promotes carcinogenesis, while loss of NF-κB results in prolonged survival and diminished tumor growth (Schwitalla et al, 2013). Constitutive Wnt activation following APC loss leads to hyperproliferation of stem cells and tumor formation via RAC1 (Ras-related C3 botulinum toxin substrate 1)-ROS-NF-κB pathway activation (Myant et al, 2013). In the small intestine, NF-κB is required for proper secretory Paneth cell differentiation and epithelial homeostasis by regulating Wnt signaling and Sox9 expression downstream of NF-κB (Brischetto et al, 2021). Recently, activation of NF-κB via ALPK1 and TIFA in proliferative intestinal cells has been linked to DNA damage and abrogated replication stress, which predisposes to mutagenesis (Bauer et al, 2020). Our data now reveal that an interplay between these two signaling pathways is in fact an integral part of antral gland physiology. Under healthy conditions, this signaling unit is restricted to the stem cell compartment. This restriction is the basis of selective immune responses if the gland becomes infected. In contrast, mutations in the Wnt signaling pathway may result in an expansion of cells with high Wnt signaling, and thus NF-κB competence, to the gland surface, where cells are more likely to be exposed to various signals from luminal bacteria. This would in turn lead to a loss of biogeographic selectivity and initiation of inflammation even by surface epithelial cells, which in turn would perpetuate the regenerative process and may contribute to tumor cell proliferation and progression.

# Materials and Methods

### Mouse experiments

All procedures that involved animals were approved by the institutional, local, and national legal authorities at the Max Planck Institute for Infection Biology (LAGeSo, Berlin, Reg. G0084/17) and were compliant with all of the relevant ethical regulations regarding animal research. Axin2^{CreErt2} mice were described before (van Amerongen et al, 2012) and were obtained from the Jackson Laboratories. Lgr4^{fl/fl} mice and Lgr5^{fl/fl} mice were kindly provided by Dr. Jan Tchorz, Novartis. Mouse models were designed for both genes by flanking exon1 with loxP elements facilitating Cre-mediated recombination and excision of exon1 including part of the 5′UTR. For Lgr4, Cre-mediated excision results in a deletion of 1.9 kb including Lgr4 exon1 plus 900 bp of 5′UTR. For Lgr5, Cre-mediated excision results in a deletion of 1.6 kb including Lgr5 exon1 plus 600 bp of the 5′UTR (Planas-Paz et al, 2016). Rspo3^{fl/fl} mice (Neufeld et al, 2012) were a kind gift from John Cobb. Myh11^{CreErt2} mice (Herring et al, 2014) were a kind gift from Stefan Offermanns. Mice that conditionally overexpress Rspo3 under the Rosa26 promoter (Rosa26Sor^{6(Cag-Rspo3)}) were described previously (Hilkens et al, 2017) and were a gift from John Hilkens and Elvira Bakker. These animals were bred with Myh11^{CreERT2} mice to generate double-heterozygous Myh11^{CreERT2}/Rosa26Sor^{6(CAG-Rspo3)} mice.

*129;129P2-ctnnb1*$^{tm(NFKBIA\Delta N)1Rsu}$ mice (*ΔN*) (Schmidt-Ullrich *et al*, 2001) and *B6-Tg(k-EGFP)3Pt/Rsu* (*k-EGFP*) (Tomann *et al*, 2016) were a kind gift from Ruth Schmidt-Ulrich.

All animals were maintained in autoclaved microisolator cages and provided with sterile drinking water and chow *ad libitum*. Six-to-eight-week-old male mice were used for this study. Sample size was estimated by own experience in this field (Sigal *et al*, 2017, 2019). Tamoxifen (Sigma) was injected intraperitoneally into mice on two to three consecutive days (4 mg 25 g$^{-1}$ bodyweight; diluted in 200 μl corn oil) at the indicated time points.

At the time of collection, the forestomach was removed, and the glandular stomach was opened along the lesser curvature and laid flat. The stomach contents were removed, and the tissue was divided into two halves along the greater curvature. For RNA analysis, the tissue was divided between antrum and corpus, and pieces were snap-frozen. For microscopy analysis, a similar longitudinal section at the midline along the greater curvature was used for all animals to minimize sampling error. For all mouse experiments, mice were randomized to experimental groups.

### *Helicobacter pylori* infection and CFU analysis

Animals were infected with a single oral dose of $1 \times 10^8$ *H. pylori* strain PMSS1 and euthanized at the indicated time points as previously described (Sigal *et al*, 2015). Longitudinal sections of stomach tissue (antrum and corpus) were weighed and then mechanically homogenized in brain-heart-infusion medium. Serial dilutions of the homogenates were plated for *H. pylori* CFU enumeration, and bacterial counts were expressed as CFU g$^{-1}$ of stomach. Lgr4$^{-/-}$ and Lgr5$^{-/-}$ mice plus littermate controls were infected with separate *H. pylori* cultures leading to variability in CFUs between two different experiments. Experiments were performed in at least three biological replicates per condition. The investigator was blinded for CFU analysis.

### Tissue processing and microscopy

Tissue samples were processed for microscopy as previously described, with minor modifications (Sigal *et al*, 2015). For paraffin embedding, tissues were fixed in 2% paraformaldehyde for 1 day. Paraffin embedding and sectioning, as well as H&E staining, were performed by the Charité Core Unit Immunopathology for Experimental Models. Paraffin-embedded sections were rehydrated, followed by an antigen retrieval step, then incubated with primary antibodies, followed by a washing step, and incubated with secondary antibody for 1 h. Samples were imaged using a Leica Sp8 confocal microscope (LAS X acquisition software) or a Zeiss Observer 7 microscope (ZEN acquisition software). The investigator performing staining was blinded for treatment and genotype.

The following antibodies were used for this study: rabbit anti-GIF (custom-made by David H. Alpers); mouse anti-Muc5ac (Invitrogen, MA5-12178, lot RL2313146B); rabbit anti-Ki67 (Cell Signaling, 9129S, clone D3B5, lot 3); rabbit anti-NF-κB p65 (Cell Signaling, D14E12, #8242, lot 16); mouse anti-E-Cadherin (BD Biosciences, 610,181); DAPI (Roche, Cat. No. 10236276001); goat anti-GFP (Abcam, ab6673); rabbit anti-CD3 (Abcam, ab16669); rabbit anti-IBA1 (VWR, 100369–764); rabbit anti-MPO (Abcam, ab208670); mouse anti-beta-catenin (Becton Dickenson, 610,153); rabbit anti-

*H. pylori* (custom-made and described previously (Sigal *et al*, 2015)); Alexa Fluor 647 Phalloidin (Invitrogen, A22287); rabbit anti-NF-κB p65 acetyl K310 (Cell Signaling, #3045); rabbit anti-Cxcl1 (Ptglab, 12335). GSII + cells were stained with Lectin GSII from *Griffonia simplicifolia*, Alexa Fluor 647 conjugate (Life Technologies, L32451, lot 1774229), nuclei were counterstained with DAPI (Roche, Cat. No. 10236276001).

### Organoid cultures

Antrum tissue was sterilized in 0.04% (w/v) sodium hypochlorite (Roth) for 15 min at room temperature, followed by 90-min incubation in buffered saline solution containing 0.5 mM DTT and 3 mM EDTA to dissociate gastric glands. Isolated glands were washed with PBS and mixed with 50 μl Matrigel (BD) and plated in 24-well plates. After polymerization of Matrigel, murine gastric culture medium (Advanced Dulbecco's Modified Eagle Medium/F12 supplemented with B-27 (Invitrogen), N-2 (Invitrogen), N-acetyl cysteine (Sigma), 100 U/ml penicillin–streptomycin (Invitrogen) and containing 50 ng ml$^{-1}$ epidermal growth factor (Invitrogen), 100 ng ml$^{-1}$ Noggin (Peprotech), 100 ng ml$^{-1}$ fibroblast growth factor 10 (Peptrotech), 10 μM gastrin (Sigma), 7.5 μM Y-27632 (Sigma), Rspo1-conditioned medium and Wnt3A-conditioned medium) was overlaid. The medium supplemented with growth factors was replaced every 2–3 days. After 2–3 days in culture, for some experiments Wnt3a and/or Rpso1 were removed or 50 ng ml$^{-1}$ BMP2 (R&D Systems) was added for a further 3–5 days. Subsequently, organoids were treated with 0.5 μM ADP heptose (Invivogen) or 10 ng/ml TNF-α (Peprotech) for 2 h. For qPCR analysis, RNA from the organoids was then extracted as described below. For immunofluorescence, organoids were fixed with 3.7% formaldehyde for 1–2 h at room temperature and embedded in paraffin as described before (Grinat *et al*, 2022).

### Microarray analysis

For microarray analysis, RNA of infected *Lgr4*$^{-/-}$ mice and the corresponding controls treated with tamoxifen 2 weeks before euthanasia were isolated from the antrum. Total RNA from bulk tissue was isolated using the RNEasy mini kit (Qiagen) following the manufacturer's protocol.

Microarray experiments were performed as independent dual-color dye hybridizations using two biological replicates. Quality control and quantification of total RNA were carried out using an Agilent 2100 Bioanalyzer (Agilent Technologies) and a NanoDrop 1,000 UV–Vis spectrophotometer (Kisker). RNA labeling was performed using the dual-color Quick-Amp Labeling Kit (Agilent Technologies). In brief, mRNA was reverse transcribed and amplified using an oligo-dT-T7 promoter primer, and the resulting complementary RNA (cRNA) was labeled with cyanine 3-CTP or cyanine 5-CTP. After precipitation, purification, and quantification, 1.25 μg of each labeled cRNA was fragmented and hybridized to whole mouse genome $4 \times 44$ K multipack microarrays (Agilent-014868, whole mouse genome $4 \times 44$ K microarray kit) according to the supplier's protocol (Agilent Technologies). Scanning of microarrays was performed with 5 μm resolution using a G2565CA high-resolution laser microarray scanner (Agilent Technologies) with extended dynamic range. Microarray image data were analyzed

using the Image Analysis/Feature Extraction software G2567AA v.A.11.5.1.1 (Agilent Technologies) using the default settings and the GE2_1105_Oct12 extraction protocol. The extracted MAGE-ML files were analyzed further using the Rosetta Resolver Biosoftware, build 7.2.2 SP1.31 (Rosetta Biosoftware). Ratio profiles comprising single hybridizations were combined in an error-weighted manner to create ratio experiments. A 1.5-fold-change expression cut-off for ratio experiments was applied together with anti-correlation of dye-swapped ratio profiles, yielding microarray analysis results that were highly significant ($P < 0.01$), robust, and reproducible (Churchill, 2002).

## GSEA analysis

We used antral stem cell signature genes (Barker et al, 2010), beta-catenin target genes (Herbst et al, 2014), and NF-κB signature genes from the MsigDB (Liberzon et al, 2015) on genes pre-ranked by gene-expression-based t-score between the antrum tissue of $Lgr4^{fl/fl}$/$Axin2^{CreErt2}$ and $Lgr4^{+/+}/Axin2^{CreErt2}$ animals using the fgsea R package (preprint: Sergushichev, 2016) with 5,000 permutations; R v. 4.0.2 was used (https://cran.r-project.org/). For each experiment, $P$-values from all gene sets were jointly adjusted for multiple testing using FDR—the method of Benjamini–Hochberg (Benjamini & Hochberg, 1995). For further information regarding GSEA and data interpretation, please refer to the original publication (Subramanian et al, 2005).

The computational code for GSEA analysis of microarray in this manuscript data can be accessed under https://github.com/Sigal-Lab/Wizenty_et_al_Lgr4_stomach_gland.

## DAVID and Revigo analysis

Genes showing significant negative changes in expression ($P < 0.05$) were analyzed by DAVID 6.7 BP direct (https://david.ncifcrf.gov). For NF-κB target genes, Gilmore database (https://www.bu.edu/nf-kb/gene-resources/target-genes/) was used to select genes showing a significant decrease in expression in Lgr4 KO ($P < 0.05$). Separate GO terms were obtained for these from DAVID 6.7 BP direct. GO terms were refined by Revigo (Uniprot mus musculus, Resnik Large; Supek et al, 2011).

## RT–PCR

For qPCR from mouse tissue, RNA was extracted from the snap-frozen antrum tissue using the RNeasy RNA Purification Kit (Qiagen). For the analysis of organoid RNA, organoids were released from Matrigel with cold Dulbecco's phosphate-buffered saline (DPBS) and pelleted by centrifugation (7 min at 4°C, 300 $g$), and RNA was then isolated using the TRIzol (Invitrogen) and the RNeasy RNA Purification Kit according to the manufacturer's protocol. Quality and quantity controls were performed for each extract using the NanoDrop 1,000 Spectrophotometer (Thermo Scientific). qPCR was performed using the Power SYBR Green RNA-to-CT 1-Step Kit (Applied Biosystems). Reactions were performed in 25 μl containing 50 ng RNA, 12.5 μl SYBR Green mix, 0.2 μl RT mix, and 0.2 μM per primer.

The cycles used were as follows: 30 min at 48°C; 10 min at 95°C; followed by 40 cycles of 15 s at 95°C; and 60 s at 60°C. For each oligonucleotide pair and RNA sample, the reaction was performed in duplicate. The expression levels of the target genes were normalized to the levels of *Gapdh* gene expression in each individual sample and expressed as fold-change compared with the expression in control tissue (WT, uninfected or nontreated), using the $2^{-\Delta\Delta Ct}$ equation (Pfaffl, 2001).

The following murine primers (Sigma) were used: *Axin2* forward 5′-TGACTCTCCTTCCAGATCCCA-3′, reverse 5′-TGCCCACACTAGG CTGACA-3′; *Ccl2* forward 5′-CAGGTCCCTGTCATGCTTCT-3′, reverse 5′-GTGGGGCGTTAACTGCATCT-3′; *Cxcl1* forward 5′-CCCAAACCGA AGTCATAGCCA-3′, reverse 5′-CTCCGTTACTTGGGGACACC-3′; *Cxcl2* forward 5′-CCCAGACAGAAGTCATAGCCAC-3′, reverse 5′-CTTCCG TTGAGGGACAGCAG-3′; *Cxcl10* forward 5′-CAAGCCATGGTCCTGA GACA-3′, reverse 5′-TGAGCTAGGGAGGACAAGGA-3′; *Gapdh* forward 5′-TCACCATCTTCCAGGAGCG-3′, reverse 5′-AAGCAGTTGGTGGTG CAGG-3′; *Gif* forward 5′-AAGCACAGCGCAAAAACTCC-3′, reverse 5′-GCAACCCCTTCATCCAAAGG-3′; *Itln1* forward 5′-GTTGCTACCA GAGGTTGCAGT-3′, reverse 5′-AGACCATCTTGTGCCTTTGTGT-3′; *Lgr4* forward 5′-TACAACTGGCTGGTAACGACC-3′, reverse 5′-GGAG GGTTAGGACTTTGAGTTCT-3′; *Lgr5* forward 5′-CCTACTCGAAGAC TTACCCAGT-3′, reverse 5′-GCATTGGGGTGAATGATAGCA-3′; *Muc5ac* forward 5′- CCTGAGGGTATGGTGCTTGA-3′, reverse 5′ TGTGTTG GTGCAGTCAGTAGAG3′; *Muc6* forward 5′-CAGCTCAACAAGGTG TGTGC-3′, reverse 5′-GGTCTCCTCGTAGTTGCAGG-3′; *Pgc* forward 5′-CCCATGGCCTATATGGATGCTT-3′, reverse 5′-CAGGCCGAACTC CTGGTTAG-3′; Sox9 forward 5′-GAGCCGGATCTGAAGAGGGA-3′, reverse 5′GCTTGACGTGTGGCTTGTTC-3′; *Tff2* forward 5′-CTGGT AGAGGGCGAGAAACC-3′, reverse 5′-CCATGACACACTGCTCCGAT-3′.

## Electrophoretic mobility shift assay (EMSA) and sodium dodecyl sulfate-polyacrylamide gel electrophoreses (SDS–PAGE)

The gel electrophoresis mobility shift assay (EMSA) is used to detect protein complexes with nucleic acids. Here, EMSA was used to determine the affinity of NF-κB to the specific sequence on DNA (the κB sequence). EMSA provides a readout of the activation state of the NF-κB pathway. The 32p radiolabeled DNA probe containing the κB sequence was incubated with the protein lysate and then separated on a gel.

EMSA was performed with whole-cell lysates (WCL). Whole-cell lysates were prepared using Baeuerle buffer (20 mM HEPES pH 7.9; 350 mM NaCl; 20% glycerol; 1 mM MgCl$_2$; 0.5 mM EDTA; 0.1 mM EGTA; 1% NP-40), including complete protease inhibitor cocktail (Roche), 10 mM NaF, 8 mM β-glycerophosphate, 0.2 mM Na$_3$VO$_4$, and 1 mM DTT. H2KκB probe from MHC promoter was used and incubated with 5 μg of whole-cell lysate for 30 min. The protein and DNA was then separated on a non-denaturing TBE-polyacrylamide gel over 90 min. The gel was vacuum dried, and signal was visualized on an X-ray film.

EMSA protocol and SDS–PAGE protocol was described previously (Mikuda et al, 2018). Supershift protocol was described previously (Kolesnichenko et al, 2021).

The following antibodies were used for this study: IκBα C-15 (Santa Cruz, sc-203), IKK-p (S176-180) (Cell Signaling, #2697), alpha-tubulin DM1A (Santa Cruz, sc- 32,293), p65 C-20 (Santa Cruz, sc-372 X), p50 E-10 (Santa Cruz, sc-8,414 X), RelB D-4 (Santa Cruz, sc-48,366 X), p52 (Millipore, 06–413), and cRel (Cell Signaling, #4727).

## Single-molecule RNA ISH

Tissue sections cut at 5 μm thickness were processed for RNA *in situ* detection using the RNAscope Red Detection Kit according to the manufacturer's instructions (Advanced Cell Diagnostics). Positive and negative control probes were used for each experiment according to the manufacturer's instructions. The following probes were used in this study: Lgr4 (Order no.: 318321, Lot: 18053A, Target region: 1973–2895); Lgr5 (Order no.: 312171, Lot: 16351A, Target region: 2165–3082).

## ScRNA-seq analysis

ScRNA-seq data from epithelial cells of murine gastric antrum were used from a published data set (Busslinger *et al*, 2021b). GEO accession number for the source data is GSE157694 (Data ref: Busslinger *et al*, 2021a). Seurat R package (Butler *et al*, 2018) was used to perform t-distributed stochastic neighbor embedding (t-SNE) analysis. t-SNE analysis was applied to visualize cell clusters. Datasets were filtered (> 50 transcripts, < 5% mitochondrial reads per cell), integrated with SCTransform to eliminate the batch effect of samples, and log-normalized, and the first 20 principal components were used to reduce dimensionality by t-SNE with a resolution of 0.1.

## Statistics

GraphPad Prism (v.8.4.0) was used for statistical analysis. Data are displayed as mean $+$ SD. $P < 0.05$ was considered to be statistically significant.

For comparison of two groups, we used an unpaired two-sided *t*-test, for multiple comparisons one-way ANOVA as indicated. Data are displayed for independent biological samples, unless otherwise indicated. The numbers are indicated in the figure legends. Microarray data displayed in Figs 3 and EV4, and Table EV1 are derived from $n = 2$ biological replicates.

# Data availability

The microarray data have been deposited in the Gene Expression Omnibus (GEO) of the National Center for Biotechnology Information under GEO accession number GSE165028 (https://www.ncbi.nlm.nih.gov/geo/query/acc.cgi?acc=GSE165028). Quantitative data that support the findings in this study are available within the paper and in the source data. All other data supporting these findings are available from the corresponding author upon reasonable request.

**Expanded View** for this article is available online.

## Author contributions

**Jonas Wizenty:** Conceptualization; data curation; software; formal analysis; validation; investigation; visualization; methodology; project administration. **Stefanie Müllerke:** Investigation. **Marina Kolesnichenko:** Software; formal analysis; investigation. **Julian Heuberger:** Investigation. **Manqiang Lin:** Investigation. **Anne-Sophie Fischer:** Investigation. **Hans-Joachim Mollenkopf:** Software; formal analysis. **Hilmar Berger:** Software; formal analysis; visualization. **Frank Tacke:** Resources; supervision. **Michael Sigal:** Conceptualization; resources; data curation; software; formal analysis; supervision; funding acquisition; validation; investigation; visualization; methodology; project administration.

In addition to the CRediT author contributions listed above, the contributions in detail are:
This study was designed by JW and MS. JW and SM performed experiments and analysis. SM performed animal experiments. MK, JH, ML, and A-SF performed experiments and provided intellectual support. H-JM performed microarray studies and HB, H-JM, and MK analyzed the microarray data. FT gave advice for experimental design and data interpretation. The manuscript was written by JW and MS; all authors provided comments.

## Disclosure and competing interests statement
The authors declare that they have no conflict of interest.

# References

van Amerongen R, Bowman AN, Nusse R (2012) Developmental stage and time dictate the fate of Wnt/beta-catenin-responsive stem cells in the mammary gland. *Cell Stem Cell* 11: 387–400

Amieva MR, El-Omar EM (2008) Host-bacterial interactions in *Helicobacter pylori* infection. *Gastroenterology* 134: 306–323

Amieva MR, Vogelmann R, Covacci A, Tompkins LS, Nelson WJ, Falkow S (2003) Disruption of the epithelial apical-junctional complex by *Helicobacter pylori* CagA. *Science* 300: 1430–1434

Arena ET, Campbell-Valois FX, Tinevez JY, Nigro G, Sachse M, Moya-Nilges M, Nothelfer K, Marteyn B, Shorte SL, Sansonetti PJ (2015) Bioimage analysis of shigella infection reveals targeting of colonic crypts. *Proc Natl Acad Sci U S A* 112: E3282–E3290

Arnold IC, Lee JY, Amieva MR, Roers A, Flavell RA, Sparwasser T, Müller A (2011) Tolerance rather than immunity protects from *Helicobacter pylori*-induced gastric preneoplasia. *Gastroenterology* 140: 199–209

Backert S, Ziska E, Brinkmann V, Zimny-Arndt U, Fauconnier A, Jungblut PR, Naumann M, Meyer TF (2000) Translocation of the *Helicobacter pylori* CagA protein in gastric epithelial cells by a type IV secretion apparatus. *Cell Microbiol* 2: 155–164

Barker N, Huch M, Kujala P, van de Wetering M, Snippert HJ, van Es JH, Sato T, Stange DE, Begthel H, van den Born M *et al* (2010) Lgr5(+ve) stem cells

drive self-renewal in the stomach and build long-lived gastric units *in vitro*. *Cell Stem Cell* 6: 25−36

Barker N, van Es JH, Kuipers J, Kujala P, van den Born M, Cozijnsen M, Haegebarth A, Korving J, Begthel H, Peters PJ *et al* (2007) Identification of stem cells in small intestine and colon by marker gene Lgr5. *Nature* 449: 1003−1007

Bauer M, Nascakova Z, Mihai A-I, Cheng PF, Levesque MP, Lampart S, Hurwitz R, Pfannkuch L, Dobrovolna J, Jacobs M *et al* (2020) The ALPK1/TIFA/NF-κB axis links a bacterial carcinogen to R-loop-induced replication stress. *Nat Commun* 11: 5117

Benjamini Y, Hochberg Y (1995) Controlling the false discovery rate: A practical and powerful approach to multiple testing. *J R Stat Soc B Methodol* 57: 289−300

Biton M, Haber AL, Rogel N, Burgin G, Beyaz S, Schnell A, Ashenberg O, Su CW, Smillie C, Shekhar K *et al* (2018) T helper cell cytokines modulate intestinal stem cell renewal and differentiation. *Cell* 175: 1307−1320.e1322

Brischetto C, Krieger K, Klotz C, Krahn I, Kunz S, Kolesnichenko M, Mucka P, Heuberger J, Scheidereit C, Schmidt-Ullrich R (2021) NF-κB determines Paneth versus goblet cell fate decision in the small intestine. *Development* 148: dev199683

Brooks P, Zur Bruegge T, Boyle EC, Kalies S, Villarreal SN, Liese A, Bleich A, Buettner M (2020) CD14 and ALPK1 affect expression of tight junction components and proinflammatory mediators upon bacterial stimulation in a colonic 3D organoid model. *Stem Cells Int* 2020: 4069354

Busslinger GA, Weusten BLA, Bogte A, Begthel H, Brosens LAA, Clevers H (2021a) Gene Expression Omnibus GSE157694 (https://www.ncbi.nlm.nih.gov/geo/query/acc.cgi?acc=GSE157694). [DATASET]

Busslinger GA, Weusten BLA, Bogte A, Begthel H, Brosens LAA, Clevers H (2021b) Human gastrointestinal epithelia of the esophagus, stomach, and duodenum resolved at single-cell resolution. *Cell Rep* 34: 108819

Butler A, Hoffman P, Smibert P, Papalexi E, Satija R (2018) Integrating single-cell transcriptomic data across different conditions, technologies, and species. *Nat Biotechnol* 36: 411−420

Castillo-Azofeifa D, Fazio EN, Nattiv R, Good HJ, Wald T, Pest MA, de Sauvage FJ, Klein OD, Asfaha S (2019) Atoh1(+) secretory progenitors possess renewal capacity independent of Lgr5(+) cells during colonic regeneration. *EMBO J* 38: e99984

Chen LF, Mu Y, Greene WC (2002) Acetylation of RelA at discrete sites regulates distinct nuclear functions of NF-kappaB. *EMBO J* 21: 6539−6548

Churchill GA (2002) Fundamentals of experimental design for cDNA microarrays. *Nat Genet* 32: 490−495

Correa P (1995) *Helicobacter pylori* and gastric carcinogenesis. *Am J Surg Pathol* 19: S37−S43

Eck M, Schmausser B, Scheller K, Toksoy A, Kraus M, Menzel T, Müller-Hermelink HK, Gillitzer R (2000) CXC chemokines Gro(alpha)/IL-8 and IP-10/MIG in *Helicobacter pylori* gastritis. *Clin Exp Immunol* 122: 192−199

Ernst PB, Crowe SE, Reyes VE (1997) How does *Helicobacter pylori* cause mucosal damage? The inflammatory response. *Gastroenterology* 113: S35−S42 discussion S50

Fast D, Petkau K, Ferguson M, Shin M, Galenza A, Kostiuk B, Pukatzki S, Foley E (2020) Vibrio cholerae-symbiont interactions inhibit intestinal repair in drosophila. *Cell Rep* 30: 1088−1100.e1085

Fischer AS, Sigal M (2019) The role of Wnt and R-spondin in the stomach during health and disease. *Biomedicine* 7: 44

Fung C, Tan S, Nakajima M, Skoog EC, Camarillo-Guerrero LF, Klein JA, Lawley TD, Solnick JV, Fukami T, Amieva MR (2019) High-resolution mapping reveals that microniches in the gastric glands control *Helicobacter pylori* colonization of the stomach. *PLoS Biol* 17: e3000231

Greicius G, Kabiri Z, Sigmundsson K, Liang C, Bunte R, Singh MK, Virshup DM (2018) PDGFRalpha(+) pericryptal stromal cells are the critical source of Wnts and RSPO3 for murine intestinal stem cells in vivo. *Proc Natl Acad Sci U S A* 115: E3173−E3181

Greten FR, Grivennikov SI (2019) Inflammation and cancer: Triggers, mechanisms, and consequences. *Immunity* 51: 27−41

Grinat J, Kosel F, Goveas N, Kranz A, Alexopoulou D, Rajewsky K, Sigal M, Stewart AF, Heuberger J (2022) Epigenetic modifier balances Mapk and Wnt signalling in differentiation of goblet and Paneth cells. *Life Sci Alliance* 5: e202101187

Harnack C, Berger H, Antanaviciute A, Vidal R, Sauer S, Simmons A, Meyer TF, Sigal M (2019) R-spondin 3 promotes stem cell recovery and epithelial regeneration in the colon. *Nat Commun* 10: 4368

Herbst A, Jurinovic V, Krebs S, Thieme SE, Blum H, Göke B, Kolligs FT (2014) Comprehensive analysis of β-catenin target genes in colorectal carcinoma cell lines with deregulated Wnt/β-catenin signaling. *BMC Genomics* 15: 74

Herring BP, Hoggatt AM, Burlak C, Offermanns S (2014) Previously differentiated medial vascular smooth muscle cells contribute to neointima formation following vascular injury. *Vasc Cell* 6: 21

Hilkens J, Timmer NC, Boer M, Ikink GJ, Schewe M, Sacchetti A, Koppens MAJ, Song JY, Bakker ERM (2017) RSPO3 expands intestinal stem cell and niche compartments and drives tumorigenesis. *Gut* 66: 1095−1105

Howitt MR, Lee JY, Lertsethtakarn P, Vogelmann R, Joubert LM, Ottemann KM, Amieva MR (2011) ChePep controls *Helicobacter pylori* infection of the gastric glands and chemotaxis in the Epsilonproteobacteria. *MBio* 2: e00098-11

Kapalczynska M, Lin M, Maertzdorf J, Heuberger J, Muellerke S, Zuo X, Vidal R, Shureiqi I, Fischer AS, Sauer S *et al* (2022) BMP feed-forward loop promotes terminal differentiation in gastric glands and is interrupted by *H. pylori*-driven inflammation. *Nat Commun* 13: 1577

Keilberg D, Zavros Y, Shepherd B, Salama NR, Ottemann KM (2016) Spatial and temporal shifts in bacterial biogeography and gland occupation during the development of a chronic infection. *mBio* 7: e01705-16

Kolesnichenko M, Mikuda N, Höpken UE, Kärgel E, Uyar B, Tufan AB, Milanovic M, Sun W, Krahn I, Schleich K *et al* (2021) Transcriptional repression of NFKBIA triggers constitutive IKK- and proteasome-independent p65/RelA activation in senescence. *EMBO J* 40: e104296

de Lau W, Barker N, Low TY, Koo BK, Li VS, Teunissen H, Kujala P, Haegebarth A, Peters PJ, van de Wetering M *et al* (2011) Lgr5 homologues associate with Wnt receptors and mediate R-spondin signalling. *Nature* 476: 293−297

Liabeuf D, Oshima M, Stange DE, Sigal M (2022) Stem cells, *Helicobacter pylori*, and mutational landscape: Utility of preclinical models to understand carcinogenesis and to direct Management of Gastric Cancer. *Gastroenterology* 162: 1067−1087

Liberzon A, Birger C, Thorvaldsdóttir H, Ghandi M, Mesirov JP, Tamayo P (2015) The molecular signatures database (MSigDB) hallmark gene set collection. *Cell Syst* 1: 417−425

Liu S, Qian Y, Li L, Wei G, Guan Y, Pan H, Guan X, Zhang L, Lu X, Zhao Y *et al* (2013) Lgr4 gene deficiency increases susceptibility and severity of dextran sodium sulfate-induced inflammatory bowel disease in mice. *J Biol Chem* 288: 8794−8803 discussion 8804

Mikuda N, Kolesnichenko M, Beaudette P, Popp O, Uyar B, Sun W, Tufan AB, Perder B, Akalin A, Chen W *et al* (2018) The IκB kinase complex is a regulator of mRNA stability. *EMBO J* 37: e98658

Myant KB, Cammareri P, McGhee EJ, Ridgway RA, Huels DJ, Cordero JB, Schwitalla S, Kalna G, Ogg EL, Athineos D *et al* (2013) ROS production and NF-κB activation triggered by RAC1 facilitate WNT-driven intestinal stem

cell proliferation and colorectal cancer initiation. *Cell Stem Cell* 12: 761–773

Neufeld S, Rosin JM, Ambasta A, Hui K, Shaneman V, Crowder R, Vickerman L, Cobb J (2012) A conditional allele of Rspo3 reveals redundant function of R-spondins during mouse limb development. *Genesis* 50: 741–749

Nigro G, Rossi R, Commere PH, Jay P, Sansonetti PJ (2014) The cytosolic bacterial peptidoglycan sensor Nod2 affords stem cell protection and links microbes to gut epithelial regeneration. *Cell Host Microbe* 15: 792–798

Parsonnet J, Friedman GD, Orentreich N, Vogelman H (1997) Risk for gastric cancer in people with CagA positive or CagA negative *Helicobacter pylori* infection. *Gut* 40: 297–301

Pfaffl MW (2001) A new mathematical model for relative quantification in real-time RT-PCR. *Nucleic Acids Res* 29: e45

Pfannkuch L, Hurwitz R, Traulsen J, Sigulla J, Poeschke M, Matzner L, Kosma P, Schmid M, Meyer TF (2019) ADP heptose, a novel pathogen-associated molecular pattern identified in *Helicobacter pylori*. *FASEB J* 33: 9087–9099

Planas-Paz L, Orsini V, Boulter L, Calabrese D, Pikiolek M, Nigsch F, Xie Y, Roma G, Donovan A, Marti P *et al* (2016) The RSPO-LGR4/5-ZNRF3/RNF43 module controls liver zonation and size. *Nat Cell Biol* 18: 467–479

Schmidt-Ullrich R, Aebischer T, Hülsken J, Birchmeier W, Klemm U, Scheidereit C (2001) Requirement of NF-kappaB/Rel for the development of hair follicles and other epidermal appendages. *Development* 128: 3843–3853

Schwitalla S, Fingerle AA, Cammareri P, Nebelsiek T, Göktuna SI, Ziegler PK, Canli O, Heijmans J, Huels DJ, Moreaux G *et al* (2013) Intestinal tumorigenesis initiated by dedifferentiation and acquisition of stem-cell-like properties. *Cell* 152: 25–38

Segditsas S, Sieber O, Deheragoda M, East P, Rowan A, Jeffery R, Nye E, Clark S, Spencer-Dene B, Stamp G *et al* (2008) Putative direct and indirect Wnt targets identified through consistent gene expression changes in APC-mutant intestinal adenomas from humans and mice. *Hum Mol Genet* 17: 3864–3875

Sergushichev AA (2016) An algorithm for fast preranked gene set enrichment analysis using cumulative statistic calculation. *bioRxiv* https://doi.org/10.1101/060012 [PREPRINT]

Shimoyama T, Crabtree JE (1998) Bacterial factors and immune pathogenesis in *Helicobacter pylori* infection. *Gut* 43: S2–S5

Sigal M, Logan CY, Kapalczynska M, Mollenkopf HJ, Berger H, Wiedenmann B, Nusse R, Amieva MR, Meyer TF (2017) Stromal R-spondin orchestrates gastric epithelial stem cells and gland homeostasis. *Nature* 548: 451–455

Sigal M, Reines MDM, Mullerke S, Fischer C, Kapalczynska M, Berger H, Bakker ERM, Mollenkopf HJ, Rothenberg ME, Wiedenmann B *et al* (2019)

R-spondin-3 induces secretory, antimicrobial Lgr5(+) cells in the stomach. *Nat Cell Biol* 21: 812–823

Sigal M, Rothenberg ME, Logan CY, Lee JY, Honaker RW, Cooper RL, Passarelli B, Camorlinga M, Bouley DM, Alvarez G *et al* (2015) *Helicobacter pylori* activates and expands Lgr5(+) stem cells through direct colonization of the gastric glands. *Gastroenterology* 148: 1392–1404.e1321

Subramanian A, Tamayo P, Mootha VK, Mukherjee S, Ebert BL, Gillette MA, Paulovich A, Pomeroy SL, Golub TR, Lander ES *et al* (2005) Gene set enrichment analysis: a knowledge-based approach for interpreting genome-wide expression profiles. *Proc Natl Acad Sci U S A* 102: 15545–15550

Supek F, Bošnjak M, Škunca N, Šmuc T (2011) REVIGO summarizes and visualizes long lists of gene ontology terms. *PLoS One* 6: e21800

Tan SH, Swathi Y, Tan S, Goh J, Seishima R, Murakami K, Oshima M, Tsuji T, Phuah P, Tan LT *et al* (2020) AQP5 enriches for stem cells and cancer origins in the distal stomach. *Nature* 578: 437–443

Tian H, Biehs B, Warming S, Leong KG, Rangell L, Klein OD, de Sauvage FJ (2011) A reserve stem cell population in small intestine renders Lgr5-positive cells dispensable. *Nature* 478: 255–259

Tomann P, Paus R, Millar SE, Scheidereit C, Schmidt-Ullrich R (2016) Lhx2 is a direct NF-κB target gene that promotes primary hair follicle placode down-growth. *Development* 143: 1512–1522

Wunder C, Churin Y, Winau F, Warnecke D, Vieth M, Lindner B, Zähringer U, Mollenkopf HJ, Heinz E, Meyer TF (2006) Cholesterol glucosylation promotes immune evasion by *Helicobacter pylori*. *Nat Med* 12: 1030–1038

Yan KS, Janda CY, Chang J, Zheng GXY, Larkin KA, Luca VC, Chia LA, Mah AT, Han A, Terry JM *et al* (2017) Non-equivalence of Wnt and R-spondin ligands during Lgr5(+) intestinal stem-cell self-renewal. *Nature* 545: 238–242

Zimmermann S, Pfannkuch L, Al-Zeer MA, Bartfeld S, Koch M, Liu J, Rechner C, Soerensen M, Sokolova O, Zamyatina A *et al* (2017) ALPK1- and TIFA-dependent innate immune response triggered by the *Helicobacter pylori* type IV secretion system. *Cell Rep* 20: 2384–2395